This is a preprint, the final version is subject to change, of the American Mineralogist (MSA)
Cite as Authors (Year) Title. American Mineralogist, in press.
DOI: https://doi.org/10.2138/am-2019-6907

REVISION 2

A comparison between the stability field of a Cl-rich scapolite and the end-member marialite

Kaléo M. F. Almeida[1*]

David M. Jenkins[1]

[1] Department of Geological Sciences and Environmental Studies

Binghamton University

Binghamton, NY, 13902

[*]Corresponding author

This is a preprint, the final version is subject to change, of the American Mineralogist (MSA)
Cite as Authors (Year) Title. American Mineralogist, in press.
DOI: https://doi.org/10.2138/am-2019-6907

Abstract

Scapolites are pervasive rock-forming aluminosilicates that are found in metamorphic, igneous and hydrothermal environments; nonetheless, the stability field of Cl-rich scapolite is not well constrained. This experimental study investigated two reactions involving Cl-rich scapolite. First, the anhydrous reaction (1) of plagioclase + halite + calcite to form scapolite modeled as: 3 plagioclase ($Ab_{80}An_{20}$) + 0.8 NaCl + 0.2 $CaCO_3$ = scapolite ($Ma_{80}Me_{20}$) was investigated to determine the effect of the Ca-rich meionite (Me = $Ca_4Al_6Si_6O_{24}CO_3$) component on the Na end-member marialite (Ma = $Na_4Al_3Si_9O_{24}Cl$). Second, the effect of water on this reaction was investigated using the hydrothermally equivalent reaction (2) H_2O + scapolite ($Ma_{80}Me_{20}$) = 3 plagioclase ($Ab_{80}An_{20}$) + $CaCO_3$ + liquid, where the liquid is assumed to be a saline-rich hydrous-silicate melt. Experiments were investigated with synthetic phases over the range of 500-1030 °C and 0.4-2.0 GPa. For reaction (1), intermediate composition scapolite shows a wide thermal stability and is stable relative to plagioclase + halite + calcite at temperatures above 750 °C at 0.4 GPa and 760 °C at 2.0 GPa. For reaction (2), intermediate scapolite appears to be quite tolerant to water; it forms at a minimum bulk salinity [X_{NaCl} = molar ratio of NaCl/(NaCl + H_2O)] of the brine of approximately 0.2 X_{NaCl} at 830 °C and 680 °C at pressures of 2.0 GPa and 1.5 GPa, respectively. Based on the study done by Almeida and Jenkins (2017), pure marialite is very intolerant to water when compared to intermediate composition scapolite. Compositional changes in the scapolite and plagioclase were characterized by X-ray diffraction and electron microprobe analysis and found to shift from the nominal bulk compositions to the observed compositions of $Ma_{85}Me_{15}$ for scapolite and to $Ab_{91}An_{09}$ for plagioclase. These results were used to model the phase equilibria along the marialite-meionite join in temperature-composition space. This study demonstrates that a small change in the scapolite composition from end-

member marialite to $Ma_{85}Me_{15}$ expands the stability field of marialite significantly, presumably due to the high entropy of mixing in scapolite, as well as increases its tolerance to water. This supports the much more common presence of intermediate scapolites in hydrothermal settings than either end-member meionite or marialite as is widely reported in the literature.

Keywords: scapolite, marialite, meionite, solid solution, chlorine, chloride brine, plagioclase

Introduction

The scapolite mineral group is a widespread rock-forming aluminosilicate and it is reported extensively in nature over a wide range of solid solution. The general formula of scapolite can be illustrated as $M_4T_{12}O_{24}A$, where the major components are M = Na and Ca, T = Si and Al, and A = Cl, CO_3, and SO_4. Minerals in the scapolite group can be regarded as the result of combining three moles of plagioclase with a salt (i.e., NaCl, $CaCO_3$, $CaSO_4$) (e.g., Evans et al., 1969; Goldsmith, 1976; Hassan and Buseck, 1988; Teertstra and Sherriff, 1997). They can be chemically represented as a solid solution of several end-members: a sodium chloride end-member, marialite ($Na_4Al_3Si_9O_{24}Cl$), two calcium carbonate end-members, meionite ($Ca_4Al_6Si_6O_{24}CO_3$) and mizzonite ($NaCa_3Al_5Si_7O_{24}CO_3$), and a calcium sulfate end-member, sulfate meionite or silvialite ($Ca_4Al_6Si_6O_{24}SO_4$) (Newton and Goldsmith, 1976; Teertstra et al. 1999). In addition, the Cl-rich component dipyre ($Na_3CaAl_4Si_8O_{24}Cl$), resulting from the substitution $Na_3Si_2Cl = Ca_3Al_2CO_3$ in meionite (Evans et al., 1969; Hassan and Buseck, 1988), may potentially be important in this study even though Teertstra and Sherriff (1997) caution that the substitutional complexity in natural scapolites precludes the clear identification of this composition as a scapolite end member. Unlike other chloride bearing minerals (such as amphiboles, micas, and apatite), scapolite contains little to no OH, thus its chemistry can be used

as a tracer of the Cl and CO_2 contents of the fluid responsible for its formation, independently of fH_2O (Ellis, 1978; Rebbert and Rice, 1997; Filiberto et al., 2014).

The relative prevalence and abundance of scapolite in metamorphic rocks and hydrothermally altered igneous rocks suggests a rather wide stability field for this mineral group (Goldsmith, 1976; Boivin and Camus, 1981; Vanko and Bishop, 1982; Mora and Valley, 1989; Lieftink et al., 1993; Kullerud and Erambert, 1999; Johnson and Barton, 2000a, 2000b). Interestingly, essentially all of the literature on natural scapolites have something in common: in all cases they are reported as solid solutions. In fact, accounts of naturally occurring scapolites approaching end-members (Cl, CO_3, and SO_4) are rare (e.g., Teertstra and Sherriff, 1997; Vanko and Bishop, 1982; Lieftink et al., 1993; Filiberto et al., 2014), suggesting that the conditions under which end-member scapolites form are rather unusual in nature.

Experimental studies reporting stability fields in pressure-temperature (*P*-*T*) space for end-member scapolites are those of Newton and Goldsmith (1976) and Almeida and Jenkins (2017). Newton and Goldsmith (1976) investigated the stability field of end-member meionite and sulfate-meionite in the $CaAl_2Si_2O_8$-$CaCO_3$ and $CaAl_2Si_2O_8$-$CaSO_4$ systems, respectively. These authors found end-member meionite and sulfate meionite to be stable at higher temperatures relative to the anorthite + salt assemblage. They reported that meionite is stable relative to anorthite and calcite above 875 °C, almost independent of pressure. On the contrary, sulfate-meionite appears to have a strong pressure dependency with the boundary located at 1.3 GPa at 1000 °C and having a negative d*P*/d*T* slope of -0.0022 GPa/°C, which restricts the conditions of its formation to high pressure (> 0.6 GPa at 1300 °C) environments. This is in agreement with the literature where scapolites with the highest sulfur content tend to come from deep-seated rocks (Lovering and White, 1964; Yoshino and Satish-Kumar, 2001; Hammerli et al., 2017).

Although Newton and Goldsmith (1976) tabulated several experiments involving marialite, they did not report a *P-T* stability field for it. Based on various observations reported in the literature, Filiberto et al. (2014) proposed a P-T diagram for marialite; however, no systematic experimental study was presented for this end-member. Almeida and Jenkins (2017) investigated the *P-T* stability field of end-member marialite in the $NaAlSi_3O_8$-NaCl and $NaAlSiO_3O_8$-NaCl-H_2O systems, for both dry and hydrothermal conditions, respectively. The main conclusions were that marialite (i) requires high-temperatures, equivalent to granulite or ultra-high-temperature (UHT) facies to be stable, and (ii) requires high NaCl concentrations, even going above the saturation level of halite in the H_2O-NaCl system, in order to be stable at hydrothermal conditions. This necessity of a high brine concentration and high temperature to stabilize end-member marialite indicates it is a "dry" mineral, and it would therefore not be likely to have a hydrothermal origin. Similar to sulfate meionite, marialite also appears to require intermediate-to-high pressures to be stable with the lowest pressure where marialite forms being 0.64 GPa at 930 °C (Almeida and Jenkins, 2017). In the presence of a concentrated brine, Almeida and Jenkins (2017) proposed the lower-pressure stability of marialite to be defined by a univariant curve starting at an invariant point at 0.8 GPa and 840 °C and having a negative d*P*/d*T* curve of -0.0025 GPa/°C.

Several researchers, including Orville (1975), Ellis (1978), and Baker and Newton (1995), have done experimental work on scapolite solid solutions. Orville (1975) determined that scapolite in the system $NaAlSi_3O_8$-$CaAl_2Si_2O_8$-NaCl-$CaCO_3$ at 750 °C and 0.4 GPa is stable relative to plagioclase + calcite + halite over the approximate range of plagioclase-equivalent (= EqAn) compositions of $EqAn_{15}$ – $EqAn_{75}$, even though albite + halite is stable relative to end-member marialite and anorthite + calcite is stable relative to end-member meionite at these same

conditions. It is worth noting that complete conversion of plagioclase to scapolite in the study of Orville (1975) was only attained in the presence of small amounts of water, and all experiments were seeded with small amounts of scapolite. The best growth of scapolite at the expense of plagioclase + salts was obtained by using excess NaCl and $CaCO_3$ and trace amounts of water. Ellis (1978) determined that solid solution scapolite is stable relative to plagioclase + calcite at 750 °C and 0.4 GPa over the range of plagioclase compositions $Ab_{47}An_{53}$ to $Ab_{17}An_{83}$. This study also confirmed that high mole fractions of NaCl in the fluid, as well as excess $CaCO_3$, are necessary to stabilize scapolite relative to plagioclase + NaCl + $CaCO_3$ over the widest range of scapolite compositions reported ($EqAn_{25}$ – $EqAn_{89}$). Baker and Newton (1995) investigated the stability field of scapolite, plagioclase, and calcite in the Cl-free system $CaAl_2Si_2O_8$-$NaAlSi_3O_8$-$CaCO_3$ at 775-850 °C and 0.7 GPa. Even though their study did not include NaCl, it does demonstrate that the incorporation of Na into meionite through a plagioclase coupled substitution, $NaSi(CaAl)_{-1}$ causes the expansion of the range of conditions over which scapolite is stable. It is suggested that the stabilization of meionite by substitution of Na for Ca and Si for Al is a consequence of the large amounts of atomic mixing possible in the scapolite structure and is primarily an entropy effect, as it has been previously described by Oterdoom and Gunter (1983). The results of Baker and Newton (1995) show a large stabilization of CO_3-rich scapolite to temperatures below the limit of pure meionite. Their results suggest that fifteen mole percent of sodium meionite component stabilizes scapolite by at least 70 °C (Baker and Newton, 1995).

The focus of this study is to investigate the pressure-temperature (*P*-*T*) stability of an intermediate composition scapolite of nominal bulk composition $Ma_{80}Me_{20}$ according to the proposed reaction:

$$3(Na_{0.8}Ca_{0.2})(Al_{1.2}Si_{2.8})O_8 + 0.8NaCl + 0.2CaCO_3 = (Na_{3.2}Ca_{0.8})(Al_{3.6}Si_{8.4})O_{24}(Cl_{0.8}(CO_3)_{0.2}) \quad (1)$$

144 plagioclase ($Ab_{80}An_{20}$) halite calcite scapolite ($Ma_{80}Me_{20}$)
145 with particular attention paid to any changes in the compositions of the plagioclase and scapolite
146 along the reaction boundary. Changes in the stability of the scapolite as water is introduced to
147 the system are also investigated, where reduction in the activity of NaCl in solution is expected
148 to destabilize the scapolite. The stability field of this Cl-rich scapolite is compared to the end-
149 member scapolites and a thermodynamic model for mixing along the marialite-meionite join is
150 proposed to enable a better understanding of Cl-rich scapolite paragenesis. It will be shown that
151 subtle changes from end-member to intermediate scapolite compositions causes a dramatic
152 expansion in its stability field. This may indicate part of the reason why solid solution scapolite
153 is commonly reported in metamorphic terrains and hydrothermal environments as opposed to
154 end-member scapolite, the latter not normally found in nature. End-member scapolites may
155 simply require temperature, pressure, and fluid compositions which are not normally attained or,
156 if they are attained at mid- to lower-crustal levels, may never have a chance to resurface for them
157 to be encountered in nature.

158 ## Methods

159 ### Starting materials

160 All phases were synthesized from appropriate mixtures of reagent-grade oxides, salt, and
161 carbonate (SiO_2, Al_2O_3, NaCl, Na_2CO_3, and $CaCO_3$). The SiO_2 was made by desiccating silicic
162 acid by heating gradually to 1100 °C in air overnight producing cristobalite. The reagents NaCl
163 and $CaCO_3$ were carefully brought to a temperature of at least 500 °C in air for several hours to
164 decrepitate aqueous fluid inclusions that are invariably present. After weighing and mixing the
165 reagents Na_2CO_3, $CaCO_3$, Al_2O_3, and SiO_2 constituting the framework components, they were
166 heated in air at 900 °C for 15 minutes to remove CO_2. The A-site salt components NaCl and

167 $CaCO_3$ were added following decarbonation. For hydrothermal experiments water was added in
168 the form of distilled water via a micro-syringe. The bulk compositions of all samples
169 investigated in this study are presented in Table 1.

170 **Sample treatment and high-pressure apparatus**

171 Starting mixtures were treated in sealed platinum and silver-palladium ($Ag_{50}Pd_{50}$)
172 capsules, which were made from tubing that was cleaned in acetone, flame-annealed to around
173 1,200 °C, and then crimped. Platinum capsules were used for synthesis experiments and were 4.0
174 mm outer diameter (OD) by 15 mm length and wall thickness of 0.18 mm. Platinum or $Ag_{50}Pd_{50}$
175 capsules were used for reversal experiments, depending on the conditions of treatment, and were
176 1.5 mm OD by 10 mm length having a wall thickness of 0.13 mm. The first set of experiments
177 focused on the synthesis of intermediate scapolite and plagioclase (i.e., $Ma_{80}Me_{20}$ and $Ab_{80}An_{20}$)
178 and about 50-60 mg of sample was used. In subsequent reversal experiments, where all desired
179 phases were present in a reversal mixture, about 5 mg of sample was used. For all the
180 experiments that were treated dry, the capsules were put in a 160 °C furnace in air for 15 minutes
181 prior to sealing to ensure that all the moisture was removed from the capsule. For hydrothermal
182 experiments, water was introduced in the form of distilled water, as mentioned above, and the
183 capsule was crimped shut, welded, and weighed. After completion of experiments the capsules
184 were reweighed to check that the capsule remained sealed. To obtain a successful yield of
185 intermediate scapolite, excess NaCl and $CaCO_3$ had to be added to the starting mixture. In order
186 to calculate accurately the brine concentrations during the hydrothermal experiments, excess
187 NaCl in the synthetic solid solution scapolite was rinsed in deionized water until it was
188 completely removed from the scapolite (except reversal mixture REVSS2). The rinsed mixture

was analyzed by X-ray powder diffraction to check that there was no NaCl left and then NaCl was reintroduced in known amounts to allow better accuracy in calculating brine concentrations.

A $^{1}/_{2}$-inch diameter, non-end-loaded piston-cylinder press was used for experiments with pressures at and above 1.0 GPa. Pressure media were made using NaCl outer sleeves, straight graphite furnaces, and either NaCl or crushable MgO inner parts around the sample, depending on the temperature. Temperatures ranged from 650 °C to 1030 °C and were measured with a chromel-alumel thermocouple with the tip placed right above the sample. Temperature uncertainties are estimated as ± 5 °C for reversal experiments (using smaller capsules with the sample within 0.5 mm of the thermocouple tip) and ± 15 °C for synthesis experiments (using larger capsules with the center of the sample within 2-3 mm of the thermocouple tip). Pressures from 1.5-2.0 GPa have estimated uncertainties of 0.05 GPa. Experiments using pressure media with NaCl inner parts were first pressurized to ~0.1 GPa below the desired pressure and then brought to the target pressure using the thermal expansion of the assemblage, usually requiring only minor bleeding off of excess pressure (hot piston-out mode). Experiments using crushable MgO inner parts experienced much less thermal expansion and were therefore pressurized to the desired pressure and required very little adjustment to the pressure during the heating phase. Temperatures were brought up from room temperature to the target temperature using heating ramps of 0.5 to 1 minute; the heating rate is noted in this study because it may have some bearing on the relative nucleation rates of scapolite versus plagioclase. After treatment between 1 and 3 days, the piston-cylinder press was quenched and the sample retrieved. The capsule was weighed, an incision was made into it, dried at 110 °C, and weighed again to determine the free-water content within the capsule.

An internally-heated gas vessel was used for the experiments performed at pressures below 1.0 GPa with argon as the pressure medium. Two Inconel®-sheathed chromel-alumel thermocouples were placed in the vessel to observe any temperature gradient along the capsule; gradients were generally 10 °C or less with corresponding uncertainties in the average temperature of ± 5 °C. Desired temperatures were reached in 3-5 minutes. Pressures were measured with both bourdon-tube and manganin-cell gauges and have an estimated uncertainty of 0.005 GPa. After between 2 and 6 days, the internally heated gas vessel was quenched, sample was retrieved, and the water content determined following the procedures described above.

Analytical Methods

Powder X-Ray diffraction (XRD) analysis was performed using a Panalytical Xpert PW3040-MPD diffractometer. Samples were mounted on a zero-background single crystal quartz plate, with the operating settings at 40 kV and 20 mA using CuKα radiation and a diffracted-beam graphite monochromator. Samples were analyzed in a continuous scan from 10 to 60° 2Θ with a step size of 0.020° at 1.0 second per step. Reaction direction was determined using the peak-area ratios of the largest peaks of scapolite [(112), 25.8° 2Θ] and plagioclase [$(\bar{2}02)$, 27.8° 2Θ] as a simple way of estimating the proportions of these phases. The Panalytical software HighScore® was used to calculate the area of selected X-ray peaks.

Reaction-reversal starting mixtures, containing all of the desired phases, were mixed three times in an agate mortar using acetone to ensure a homogeneous mixture. Next, the mixtures were scanned from 20 to 31° 2Θ five times to acquire an average and standard deviation of the peak-area ratios for reference; reaction direction was then achieved by comparing peak-area ratios observed in subsequent treatments of the starting mixture to these reference ratios. Unit-cell dimensions were determined by Rietveld structure refinement using

the program GSAS (Larson and Von Dreele, 2000). The zero point of 2Θ was refined using NaCl (a_0 = 5.6401 Å) either present in the scapolite samples or added to the plagioclase samples as an internal standard to account for differences in sample displacement from one scan to another. Refinements were initiated using the structures of albite and marialite reported by Prewitt et al. (1976) and Sokolova et al. (1996), respectively. Parameters that were refined included background (function 1, shifted Chebyschev), scale factors, unit-cell dimensions, preferred orientation (100 axis, for halite), and LX terms in the profile function.

Electron probe micro-analysis (EPMA) was done on a JEOL 8900 Superprobe. Samples were mounted in epoxy, polished to a final diamond grit size of 0.5 μm, carbon coated, and analyzed using beam conditions of 15 kV and 10 nA. Noticeable decreases in the count rates of Na for both plagioclase and scapolite were observed after exposure to the electron beam for more than 20 s; therefore, analyses were done using 10 seconds on peaks and 3 seconds on background to minimize the effects of Na diffusion under the electron beam. No decrease in the count rates for Cl were observed for scapolite. Matrix corrections were made using the atomic number, absorption, and fluorescence (ZAF) correction scheme (e.g., Reed, 1996, p. 134–140). The standards used were: albite for Na, wollastonite for Ca, palladium chloride ($PdCl_2$) for Cl, and pure oxides for Si and Al.

Results

Synthesis and characterization of starting phases

Starting phases were synthesized in a temperature range of 700-1030 °C and 0.4-1.8 GPa for 1 to 6 days. The bulk compositions of the mixtures and synthesis conditions are listed in Table 1. In order to obtain high yields of Cl-rich scapolite three factors were considered necessary: (a) maintenance of a high stoichiometric proportion of NaCl and $CaCO_3$ in the starting mixture, (b)

use of a relatively rapid heating time from room temperature to the target temperature (i.e., ramp time) in order to prevent plagioclase nucleation during heating, and (c) use of high temperatures. Generally, NaCl and $CaCO_3$ had to be introduced in excess to produce a substantial yield of Cl-rich scapolite (≥ 80 wt%) using ramp times of 0.5-1.0 minute (i.e., heating rates of 343-172 °C/s). Although the highest and purest yields of plagioclase were obtained in the internally heated gas vessel at lower pressures under hydrothermal conditions, samples SSM1-1P and SSMF1-10, both of which were prepared with the intent to produce scapolite at 900 °C and 1.5GPa with the shorter ramp time (Table 1), yielded plagioclase along with excess halite and calcite. From this we can conclude that temperature, rather than the ramp time, played a larger role and was not sufficient to stabilize scapolite. High yields of intermediate scapolite were obtained at higher temperature conditions with longer ramp time. Generally, the synthetic scapolite and plagioclase are equant grains with average sizes of 2-5 μm, but some grains get up to 30-50 μm in plan view and exhibit no apparent reaction textures (e.g., grain armoring or zonation). Figure 1a is a representative back-scattered electron image of synthetic plagioclase while Figure 1b is that of a reaction-reversal starting mixture.

Compositions of the starting material scapolite and plagioclase were obtained by electron microprobe analysis of individual grains. These data are summarized in Table 2 and shown as the solid symbols in Figures 2a,b; the complete set of electron microprobe analyses are available as supplementary data. The relatively large uncertainties in the observed compositions are attributed in part to the small grain sizes and diffusion of Na under the electron beam. Despite this uncertainty, the observed average compositions of both scapolite and plagioclase are in general not the intended or nominal compositions of 0.20 mole fraction of Ca/(Ca+Na). With the exception of the plagioclase used in the higher-temperature experiments in Figure 2b (SSM1FP-

4), which is within the 1σ uncertainties of the intended composition, the remainder of the starting materials are shifted to lower Ca contents. The Ca content of the plagioclase used in the lower-temperature experiments (SSM1-10) is decidedly depleted in Ca, presumably owing to the nucleation of wollastonite (Fig. 1a). Starting material scapolite (SSMF3-3, SSMF3-7) is similarly depleted in Ca which is attributed to the preferential partitioning of Ca into minor amounts of coexisting aluminosilicate and wollastonite not observed in XRD patterns but observed under the electron microprobe. Though these compositional shifts in the starting material scapolite and plagioclase were unintended, this actually provides some means for determining whether or not compositional re-equilibration occurs in these phases during the reversal experiments, as discussed below.

To provide an independent check on the compositions of plagioclase, their compositions were estimated from the unit-cell dimension vs composition relations presented in Benesek et al. (2003) for synthetic (high) plagioclase. Of the cell dimensions given, the angle β appears to have the greatest dependence on composition. Therefore, a third-order polynomial was fit to the data of Benisek et al. (2003) for plagioclase ranging from $An_0 - An_{70}$, which is given in Table 2. Plagioclase compositions derived from this expression (Table 2) are broadly consistent with the microprobe analyses, indicating that the shifts in starting material compositions are not an artifact of the analytical technique.

The degree of Al-Si order/disorder in plagioclase for this study has been determined using the unit-cell angle γ (°) calibrated as a function of composition and Al ordering at the t_1O site by Kroll and Ribbe (1980). The degree of ordering is determined by the parameter $t_1O - \langle t_1m \rangle$, with the theoretical range of 0 to 1 for fully disordered or ordered plagioclase, respectively; however, in practice the lowest value is about 0.04 indicating the persistence of at least minor

ordering in albite even after heating 40-60 d near its melting temperature (1060-1080 °C). Correction for the plagioclase composition was taken from the microprobe analyses. The observed values of $t_1O - \langle t_1m \rangle$ are given in Table 2 and range between 0.16-0.21. This indicates the presence of substantial disorder; however, its nearly constant value suggests changes in Al-Si ordering is not likely to be an important factor in the phase equilibria observed here.

Stability of Cl-rich scapolite at dry conditions

Synthesis products containing strong yields of scapolite and plagioclase were mixed together to acquire a well-seeded reversal mixture for investigating reaction (1). Thus, equilibrium is demonstrated by the growth of scapolite at the expense of plagioclase, halite, and calcite with increasing temperature and vice versa with decreasing temperature with minimum influence from phase–nucleation kinetics (Almeida and Jenkins, 2017). Table 3 lists the synthesis products used to make the reversal mixtures.

A series of experiments at dry conditions was done over the range of 500-1000 °C and 0.4-2.0 GPa for 1 to 4 days. The results of these experiments are given in Table 4 and shown in Figure 3. The solid line that is shown is a straight-line interpretation of the experimental data fit "by eye." Shown for comparison is the lower-thermal stability of end-member marialite reported by Almeida and Jenkins (2017). As discussed in detail below, the compositions of the coexisting scapolite and plagioclase are $Ma_{85}Me_{15}$ and $Ab_{91}An_{09}$, respectively, indicating minor enrichment in the sodic components. What is most striking about Figure 3 is the pronounced expansion in the stability field of this intermediate composition scapolite compared to end-member marialite. In other words, the intermediate composition scapolite is stable to much lower temperatures than end-member marialite.

Besides having a lower thermal stability, this intermediate scapolite also appears to be stable at lower pressures compared to marialite. Though the experimental data are limited owing to sluggish reaction rates for these dry experiments, the lower-pressure data show that scapolite can be stable at 0.4 GPa and 750 °C as opposed to marialite that is only stable at or above 0.64 GPa. A possible lower-pressure stability limit, modeled after that of marialite, is shown in Figure 3 by the queried dashed line. It should be noted that experiments involving mixture REVSS1 are reported in Table 4 and the results involving this mixture are broadly consistent with those obtained with mixture REVSS2. However, they were eventually not included in constructing the *P-T* diagram due to minor amounts of wollastonite present in this mixture, coming from the plagioclase (SSM1F-1) used in this mixture, that could possibly compromise the results near the reaction boundary. They are included in Table 4 as supporting evidence for the placement of the univariant boundary shown in Figure 3.

Stability of Cl-rich scapolite at hydrothermal conditions

It is of interest to determine how scapolite formation is affected by the presence of water which will preferentially dissolve halite and should, at some concentration, cause scapolite to break down as the activity of NaCl in the ambient brine decreases. Analogous to the results reported by Almeida and Jenkins (2017) for end-member marialite, introduction of water is expected to de-stabilize the intermediate scapolite of reaction (1) as a result of the approximate reaction:

$$(Na_{3.2}Ca_{0.8})(Al_{3.6}Si_{8.4})O_{24}(Cl_{0.8}(CO_3)_{0.2}) + xH_2O = 3\ (Na_{0.8}Ca_{0.2})(Al_{1.2}Si_{2.8})O_8 + 0.2\ CaCO_3 + 0.8\ NaCl{\cdot}xH_2O\ (NaCl_{liq}) \quad (2)$$

scapolite ($Ma_{80}Me_{20}$) water plagioclase ($Ab_{80}An_{20}$) calcite

where $NaCl_{liq}$ is dominantly a NaCl-H_2O brine but likely with minor amounts of silicate, calcium carbonate, and water dissolved in it. This has been suggested by Eugster and Protska (1960) and supported by the study of Makhluf et al. (2016) on the system $NaAlSi_3O_8$-H_2O-NaCl at 1.0 GPa, where the latter study demonstrated at least minor (~1 wt%) albite dissolved in brines with up to 0.2 mole fraction of NaCl.

Two experiments were done with the equilibrium-reversal starting mixture REVSS2 while the remaining experiments were done with REVSS4 and REVSS5. For the latter two mixtures, any NaCl that was originally present from the scapolite synthesis was rinsed out of the samples and reintroduced in known amounts to improve the precision of the calculated brine concentrations. After rinsing samples REVSS4 and REVSS5, 4 moles of NaCl and 0.8 moles of $CaCO_3$ per mole of scapolite were added to each of them. Experiments at hydrothermal conditions were done over the range of 660-850 °C and 1.5-2.0 GPa varying in length from 1-2 days with the results given in Table 5 and shown in Figures 4a,b. Figures 4a and 4b show the T-X_{NaCl}^{Bulk} diagrams at fixed pressures of 2.0 and 1.5 GPa, respectively, where X_{NaCl}^{Bulk} indicates the mole fraction of NaCl/(H_2O + NaCl) for the bulk mixture which may not necessarily be the true composition of the liquid phase. Because neither scapolite nor plagioclase incorporate significant amounts of water, the general configuration of Figures 4a and 4b should have a flat boundary starting at X_{NaCl}^{Bulk} = 1.0, corresponding to the location of this reaction determined from the dry experiments, and extending isothermally left to lower brine concentrations until the concentration of NaCl reaches a value where scapolite is no longer stable at this temperature. The estimated hydrothermal halite liquidus or saturation boundaries extrapolated from lower-pressure results of Aranovich and Newton (1996) are shown here for reference.

From Figures 4a,b one can see that scapolite is stable in brines as low as 0.2 $X_{\mathrm{NaCl}}^{\mathrm{Bulk}}$ at 2 GPa and perhaps as low as 0.15 $X_{\mathrm{NaCl}}^{\mathrm{Bulk}}$ at 1.5 GPa, though the uncertainty in the breakdown of scapolite at this pressure suggests a value as high as 0.3 as indicated by the dashed line. It appears that this intermediate composition scapolite is much more tolerant of water compared to end-member marialite. For instance, a minimum bulk salinity of 0.8 is needed at 2.0 GPa and 1050 °C to stabilize marialite (Almeida and Jenkins, 2017), which is well above the (extrapolated) halite saturation boundary at these conditions. Unlike marialite, intermediate scapolite remains stable all the way over to the halite saturation curve at 2 GPa (Fig. 4a) and near or at the saturation curve at 1.5 GPa (Fig. 4b).

The degree of order/disorder in the plagioclase formed in reaction (2) was examined for several samples which had strong plagioclase growth. Plagioclase in REVSS4-4 treated at the higher temperature of 830 °C gave a $\Delta(131)$ value of 1.92 and γ of 89.91(2)° indicating it remained largely disordered with corresponding values of $t_1O - \langle t_1m \rangle$ being 0.123 and 0.189, respectively. Plagioclase in REVSS5-2 grown at the lower temperature of 680 °C gave a $\Delta(131)$ value of 1.83 and γ of 89.78(2)°, both parameters giving $t_1O - \langle t_1m \rangle$ of 0.245 for $X_{An} = 0.10$. This represents a minor degree of ordering compared to the initial plagioclase (0.211), though considerably less than the nearly complete ordering ($\Delta(131) = 1.15$, $t_1O - \langle t_1m \rangle = 0.95$) expected even for pure albite at this temperature and pressure (Goldsmith and Jenkins, 1985). In general, the plagioclase has remained largely disordered and represents little change from the starting plagioclases (SSM1FP-4, SSM1-10, Table 2).

Cl-rich scapolite and plagioclase compositions

The compositions of coexisting scapolite and plagioclase participating in reaction (2) were determined from the hydrothermal experiments, where the presence of water is expected to

enhance reaction rates and promote larger grain sizes to facilitate microprobe analysis. Scapolite and plagioclase compositions from selected reversal experiments were determined via EPMA, and the average values are listed in Tables 6 and 7, respectively. The full set of microprobe analyses are available in the supplemental table.

For scapolite, the same approach for cation calculation used by Evans (1969), Lieftink et al. (1993), and Teertstra and Sherriff (1997) was applied in this study. The formula of scapolite was calculated by normalizing to Si + Al = 12 atoms per formula unit (apfu). The criteria for accepting the analysis was based on (1) the analytical weight-percent total from the EPMA analysis being above 80 wt%, which is well above the 65 wt% minimum determined by Giblin et al. (1993), and (2) the sum of all cations being 16.0 ± 0.2. The former criterion provides the first-order filter for accepting an analysis of a grain that may be smaller than the electron-beam excitation volume, where previous studies (e.g., Solberg et al., 1981; Giblin et al., 1993; Jenkins and Corona, 2006) have shown that correct cation proportions can be preserved for analyses as low as 60-65 wt%. The latter criterion filters out analyses that simply do not have the correct stoichiometry as imposed by the crystal structure. It was difficult to obtain samples that obeyed the second criterion for the scapolite, for reasons that are unclear. One possibility is that the electron beam is analyzing overlapping and different minerals, but another complicating factor is the rapid Na diffusion under the electron beam, even for the relatively short counting times used in this study. This diffusive loss of Na under the electron beam was also described by Vanko and Bishop (1982) for the analysis of marialitic scapolite. Therefore, compositions could show a slight deficit in Na and corresponding relative increase in Al and Si. In an attempt to minimize Na diffusion, the current on the electron microprobe was reduced to 2 nA and the analyses were done using counting times of only 3 seconds on peaks and 1 second on the background and using

a 2 μm spot size. The analyses still showed a lot of scatter; however, those analyses that adhered to the selection criteria confirmed the compositions obtained under the normal higher current and longer counting times indicated in the Methods section. Although the error bars are large, Figure 2a shows a systematic shift from the Na-rich starting compositions (solid circles, triangle) to a composition which, on average, has Ca/(Ca+Na) of 0.15 (open circles, triangle) with a corresponding scapolite composition of $Ma_{85}Me_{15}$.

The criteria for accepting the analysis of plagioclase was based on (1) having an analytical total above 80 wt%, which is the same as that used for scapolite, and (2) the sum of all cations were 5.0 ± 0.1 on the basis of 8 oxygens [albite (Ab) and anorthite (An) being $NaAlSi_3O_8$ and $CaAl_2Si_2O_8$, respectively]. Albite mole fractions (X_{Ab}) were determined both by the Na-Ca ratio and Si-Al content as indicated in the footnote to Table 7, and both methods were in close agreement. Figure 2b shows a systematic shift for the higher-temperature experiments, which used the plagioclase SSM1FP-4 (solid square), to plagioclase with slightly lower Ca contents (open squares). In contrast, the lower-temperature experiment used the Ca-poor plagioclase SSM1-10 (solid diamond) which showed a slight enrichment in Ca (open diamond). Taken together, the plagioclase shows an equilibrium composition of about $Ab_{91}An_{09}$, which was approached from both directions.

Both the scapolite and plagioclase equilibrium compositions are shifted from the intended or original bulk compositions of $Ma_{80}Me_{20}$ and $Ab_{80}An_{20}$, respectively. This is most noticeable for the plagioclase. The deficient An content can be accounted for by the presence of minor wollastonite, corundum, and quartz (Fig. 1a, Table 1) which when summed together constitute anorthite. The coexistence of quartz and corundum clearly indicates that this is a metastable assemblage that presumably results from the rapid nucleation of these phases relative to

plagioclase. Scapolite is much closer to the intended bulk composition; however, minor amounts of coexisting non-scapolite phases (aluminosilicate and wollastonite, together equivalent to anorthite) were observed during microprobe analysis even if they were insufficient to appear in the powder XRD patterns.

In view of the above discussion, a more realistic representation of reaction (2) occurring in the hydrothermal experiments can now be formulated that includes both the observed compositional shifts in the scapolite and plagioclase as well as the minor additional phases. Because the minor coexisting phases (wollastonite, aluminosilicate, etc.) can sum up to the equivalent of anorthite (an_{equiv}), one can re-balance reaction (2) by allowing a certain proportion of the plagioclase, up to 0.2 an_{equiv} in this case, to be exsolved as these minor phases. The following reaction is balanced on the basis of one mole of scapolite of the composition $Ma_{85}Me_{15}$:

$$(Na_{3.4}Ca_{0.6})(Al_{3.45}Si_{8.55})O_{24}(Cl_{0.85}(CO_3)_{0.15}) + yH_2O = 2.8(Na_{0.91}Ca_{0.09})(Al_{1.09}Si_{2.91})O_8 +$$

scapolite ($Ma_{85}Me_{15}$) water plagioclase ($Ab_{91}An_{09}$)

$$(0.20 - x)(CaSiO_3{+}SiO_2{+}Al_2O_3) + 0.15CaCO_3 + [0.85NaCl{\cdot}x(CaSiO_3{+}SiO_2{+}Al_2O_3){\cdot}yH_2O]$$

an_{equiv} calcite $NaCl_{liq}$ (3)

where the components in parentheses are the minor phases stoichiometrically equivalent to anorthite (an_{equiv}) and x refers to the proportions of these components, along with y moles of water, incorporated into the NaCl-rich liquid ($NaCl_{liq}$). The stoichiometric proportions of NaCl and $CaCO_3$ in reaction (3) are based on the ideal compositions of end-member marialite and meionite, which, at least for NaCl, is fairly close to the average Cl content (= 0.89 ± 0.09 apfu) of the scapolites reported in Table 6.

Discussion

Compositions of synthetic scapolite

Figure 5a shows the compositions of the synthetic scapolite (solid squares) equilibrated along the univariant curve of reaction (3) as reported in Table 6. Also shown for comparison are the compositions of 109 natural scapolites selected from the literature that are relatively SO_3 poor and that span a wide range of scapolite-composition space. As can be seen in Figure 5a, scapolite compositions do not follow any one binary end-member join. Near the Cl-rich portion of this diagram, and certainly within the analytical uncertainties, the scapolites formed in this study are fairly well represented by the join marialite-meionite. This choice of scapolite components is also supported by Teertstra and Sherriff (1997) who, after an extensive review of the literature available at that time, noted the complexity of solid solutions in the scapolites and indicated two possible alternatives that may control the chemical composition of scapolites. The first alternative suggests that in closed systems with a low fluid/rock ratio, variations in X_{Cl} of scapolite may be preserved in metamorphic rocks on a scale of cm, suggesting that scapolite composition is a sensitive indicator of NaCl activity in coexisting fluid. The second one suggests that Cl content of scapolite is rather strongly controlled by the crystal structure, and that the chlorinity of the coexisting fluid is a secondary factor after charge-balance constraints imposed by the framework. Nonetheless, their study suggested marialite and meionite as the solid solution providing the best overall representation for NaCl-rich scapolites.

In view of the potential Cl enrichment in the synthetic scapolite, an additional plot is provided in Figure 5b to help gauge whether the scapolite component dipyre ($Na_3CaAl_4Si_8O_{24}Cl$) may be a significant component in the synthetic and natural Cl-rich scapolites, as trends toward the Na-rich and CO_3-free portion of the series have been reported previously. For instance, Lieftink et al. (1993) reported Cl-rich scapolites from Bamble, Norway, with 3.7 Al apfu (rather

than 3.0 Al apfu, as expected for end-member marialite) for an A site fully occupied by Cl, suggesting a high proportion of the dipyre component. However, as seen in Figure 5b, there is considerable scatter of the data between marialite and dipyre, even for this sampling of published scapolite analyses, making it difficult to identify any clear trend favoring one of these end-members over another. Figures 5a and 5b together suggest that mizzonite is a reasonable choice as a carbonate-rich component; unfortunately there are no thermochemical data for mizzonite. Indeed, there are no thermochemical data for any scapolites other than meionite and the recent data for marialite of Almeida and Jenkins (2017). Until additional data on other scapolite end-members are available, the marialite-meionite join will be adopted as a reasonable representation of the compositional variations in scapolite, particularly near the Cl-rich end.

Cl-rich scapolite *P-T* phase equilibria

Results on the stability of the intermediate scapolite studied here can be compared with earlier results on end-member meionite from Newton and Goldsmith (1976) and on marialite from Almeida and Jenkins (2017) to illustrate how the addition of minor meionite affects the *P-T* stability of marialite. Figure 6 shows the lower-thermal stability of the scapolite investigated in this study ($Ma_{85}Me_{15}$) in comparison to that of the end-member scapolites marialite ($Ma_{100}Me_{0}$) from Almeida and Jenkins (2017) and meionite ($Ma_{0}Me_{100}$) from Newton and Goldsmith (1976). There is a pronounced expansion (~300 °C at 1.5 GPa) in the stability of scapolite arising from the 15 mol% substitution of meionite into marialite. This phenomenon is attributed to the greater entropy of mixing in scapolite relative to plagioclase. Based on the mineral analyses shown in Figure 2, there does not appear to be any obvious variatoin in mineral compositions along this univariant boundary such that this boundary is essentially an isopleth of constant scapolite composition.

Marialite-meionite *T-X* phase equilibria

By combining the information on the intermediate scapolite of this study with the *P-T* stability of end-member marialite from Almeida and Jenkins (2017) and meionite from Goldsmith and Newton (1977) and the extant thermochemical data for these end members, it is possible to calculate the temperature-composition (*T-X*) phase equilibria for the marialite-meionite join in equilibrium with plagioclase. The major challenge in calculating a *T-X* diagram is the lack of information on the activity-composition relations for scapolite and the limited experimental data to constrain any proposed activity models. With this in mind, simplistic activity expressions for the Ma and Me components in scapolite are used here which are sufficient to give the general configuration of the diagram, but which will surely need revision as additional data become available.

Using an activity model involving random mixing on all sites (e.g., Price, 1985) for scapolite produces activities that are dependent on the mole fraction (*X*) of site occupancy that varies as X^{17} which, in turn, yields extremely small activities with attendant small differences in Gibbs free energies making it challenging to calculate boundaries between coexisting phases. Instead, activity expressions that involve coupled substitutions or restricted mixing arising, for example, from Al avoidance in anorthitic plagioclase (e.g., Kerrick and Darken, 1975), were adopted here. Based on the crystallographic study of scapolites along the marialite-meionite join by Sokolova and Hawthorne (2008), the majority of cation substitution occurs on the four *T*(1) sites, which range from fully occupied by Si in marialite to approximately 50% occupancy by Si and Al for meionite. Assuming random mixing of Al and Si on these four *T*(1) sites and coupled substitutions with the cations and anions in the remaining *T*(2), M, and A sites, one has the ideal activities:

530 $$a_{\mathrm{Ma}}^{\mathrm{Ideal}} = X_{\mathrm{Si}}^{4} = X_{\mathrm{Ma}}^{4} = X^{4} \quad (4a)$$

531 $$a_{\mathrm{Me}}^{\mathrm{Ideal}} = 4(1-X)^{2}\left(\frac{1+X}{2}\right)^{2} \quad (4b)$$

532 Non-ideal mixing is accounted for using a macroscopic two-parameter (asymmetric) Margules
533 treatment calibrated to the plagioclase and scapolite compositions from this study at 680 °C and
534 1.5 GPa. The associated activity coefficient γ_i for component *i* is calculated as:

535 $$RT\ln(\gamma_{\mathrm{Ma}}) = (1-X_{\mathrm{Ma}})^{2}[W_{\mathrm{Ma}} + 2(W_{\mathrm{Me}} - W_{\mathrm{Ma}})X_{\mathrm{Ma}}] \quad (5a)$$

536 $$RT\ln(\gamma_{\mathrm{Me}}) = (1-X_{\mathrm{Me}})^{2}[W_{\mathrm{Me}} + 2(W_{\mathrm{Ma}} - W_{\mathrm{Ms}})X_{\mathrm{Ma}}] \quad (5b)$$

537 where W_{Ma} and W_{Me} are the interaction parameters for the asymmetric treatment. These are
538 multiplied by the ideal activities to obtain the real activities, i.e., $a_i = a_i^{\mathrm{Ideal}} \cdot \gamma_i$. The
539 thermodynamic treatment of high structural state plagioclases from Newton et al. (1980) was
540 used for the albite-anorthite join. The complete set of thermodynamic data and expressions used
541 to calculate the *T*-*X* diagrams presented here is given in Appendix 1.

542 The calculated phase boundaries and derived values of W_{Ma} and W_{Me} calibrated to the two
543 data points from this study at 1.5 GPa are shown in Figure 7a. Of particular note is the
544 pronounced expansion of the scapolite stability field relative to plagioclase, similar to the *T*-*X*
545 diagrams of Oterdoom and Gunter (1983) and Baker and Newton (1995) for the carbonate
546 scapolites. The large negative interaction parameter derived in this study is also consistent with
547 the large negative (regular solution) interaction parameters derived in the former studies.

548 Using the same ideal activities proposed in equations (4a,b), one can estimate interaction
549 parameters that model, at least approximately, the T-X correlations observed for a variety of Cl-
550 and CO_3-rich scapolites coexisting with plagioclase as reported from different localities. Shown
551 in Figure 7b are coexisting scapolite (solid symbols) and plagioclase (open symbols) from

552 metamorphosed argillaceous limestones from the Chiavenna complex, Italy (Oterdoom, 1979;
553 Oterdoom and Gunter, 1983), calc-silicate units of the Wallace Formation, northern Idaho
554 (Rebbert and Rice, 1997), metagabbro from the Adirondack Mountains, NY (Johnson et al.,
555 2004), and granitic gneiss from the Munali hills area of the Lufilian-Zambezi belt, Zambia
556 (Katonga et al., 2011). Interaction parameters were derived from the approximately average
557 compositions of coexisting plagioclase and scapolite for the Ca-poor (Cl-rich) phases, and the
558 phase boundaries were calculated using the same thermodynamic treatment as used in Figure 7a.
559 What is surprising is how well the Ca-rich samples are modeled by this treatment even though
560 they were not included in deriving the interaction parameters. There are obvious inconsistencies
561 between the boundaries modeled here and the trends shown by the field data in Figure 7b,
562 particularly regarding the Ca-poor samples which appear to have increasing Ca contents with
563 increasing *T*; however, the phase relations given in Figure 7b are offered as a starting point for
564 quantifying scapolite-plagioclase phase equilibria along the marialite-meionite join.

565 **Implications**

566 Scapolites occur in many metamorphic terrains and metasomatic environments (Vanko and
567 Bishop, 1982; Mora and Valley, 1989; Teertstra and Sherriff, 1997; Johnson and Barton, 2000a,
568 2000b; Johnson et al., 2004; Katongo et al., 2011; Hammerli et al. 2014). The overwhelming
569 majority of scapolites are intermediate in composition (Teertstra and Sherriff, 1997) and only
570 rarely do they approach end-member compositions, such as the Cl-rich scapolite in melt
571 inclusions in the martian meteorite Nakhla (Filiberto et al., 2014). Understanding the *P-T-X*
572 conditions under which Cl- and CO_3-bearing scapolite forms may help to explain the prevalence
573 of intermediate, as compared to end member, scapolites. The results from this study demonstrate
574 that a small change in the scapolite composition from end-member marialite to intermediate

scapolite ($Ma_{85}Me_{15}$) causes a shift in its stability, relative to the plagioclase plus salt assemblage, by 260 °C from 990 ° to 730 °C at 2.0 GPa. This greatly expanded scapolite stability field is illustrated in Figures 7a and 7b. Furthermore, the intermediate scapolite is much more tolerant to lower brine salinities. For instance, the intermediate scapolite of this study requires only a brine salinity of approximately 0.2 $X_{\mathrm{NaCl}}^{\mathrm{Bulk}}$ (near halite saturation) at 830 °C and 680 °C at pressures of 2.0 GPa and 1.5 GPa, respectively, in order for it to be stable. In comparison, pure marialite is very intolerant to water; it requires a minimum brine salinity of about 0.8 $X_{\mathrm{NaCl}}^{\mathrm{Bulk}}$ (which is *above* halite saturation) at 1050 °C and 1000 °C at pressures of 2.0 GPa and 1.5 GPa, respectively, to stabilize marialite. Although this experimental study was mostly performed at relatively high pressures replicating lower crust conditions, one experimental run (REVSS2-10) indicated that intermediate scapolite was stable at pressure as low as 0.4 GPa and 750 °C. This suggests that if a closed system has an abundant source of Na and Cl (i.e. evaporitic sediments or brines), marialitic scapolite could be stable at upper and middle crustal conditions. Some geological settings that could contain Cl-rich scapolite formed from high-salinity brines at lower pressure conditions are mid-ocean ridge hydrothermal systems (Alt, 1995; Fontaine et al., 2007), zones of back-arc spreading (Kendrick et al., 2014), or even igneous intrusions into continental basins containing evaporites (Vanko and Bishop, 1982). The results from this study are consistent with those of Ellis (1978) who found that intermediate scapolites, and not end-member marialite or meionite, are stable at 750 °C and 0.4 GPa in the presence of a wide range of bulk brine salinities. The combined effects of a broader thermal stability field and tolerance to lower salinities mean that intermediate scapolites will be more commonly encountered in shallow- to mid-crustal levels at temperatures of ~500 °C (~800 K) or higher.

Acknowledgments

The manuscript was much improved by the careful reviews of J. Filiberto and an anonymous reviewer and the editorial handling of S. Penniston-Dorland. The authors are grateful to David Collins who assisted with the electron microprobe analyses. Financial support for this study came from NSF grant EAR-1347463 to D.M.J.

Appendix

The following thermodynamic expressions were used to calculate the phase diagrams shown in Figures 7a and 7b. The reactions defining the stability of the components $Na_4Al_3Si_9O_{24}Cl$ (= Ma) and $Ca_4Al_6Si_6O_{24}CO_3$ (= Me) in scapolite relative to $NaAlSi_3O_8$ (= Ab) and $CaAl_2Si_2O_8$ (=An) in plagioclase are:

$$3\ NaAlSi_3O_8 + NaCl = Na_4Al_3Si_9O_{24}Cl \qquad \text{A1}$$

$$3\ CaAl_2Si_2O_8 + CaCO3 = Ca_4Al_6Si_6O_{24}CO_3 \qquad \text{A2}$$

The equilibrium constants corresponding to these reactions are:

$$K_1 = \frac{a_{\mathrm{Ma}}^{\mathrm{Scap}}}{\left(a_{\mathrm{Ab}}^{\mathrm{Plag}}\right)^3} \qquad \text{A3}$$

$$K_2 = \frac{a_{\mathrm{Me}}^{\mathrm{Scap}}}{\left(a_{\mathrm{An}}^{\mathrm{Plag}}\right)^3} \qquad \text{A4}$$

where a_i^j is the activity of component *i* in phase *j*. Substituting the activity-composition relations indicated in equations 4a and 4b for scapolite, the activity coefficients in 5a and 5b for scapolite, and the activity-composition expressions of Newton et al. (1980) for plagioclase into A3 and A4, one has:

$$K_1 = \frac{X_{\mathrm{Ma}}^4 \cdot \gamma_{\mathrm{Ma}}}{\left(X_{\mathrm{Ab}}^2 (2 - X_{Ab}) \cdot \gamma_{\mathrm{Ab}}\right)^3} \qquad \text{A5}$$

This is a preprint, the final version is subject to change, of the American Mineralogist (MSA)
Cite as Authors (Year) Title. American Mineralogist, in press.
DOI: https://doi.org/10.2138/am-2019-6907

$$K_2 = \frac{\left(4(1-X_{\mathrm{Ma}})^2\left(\frac{1+X_{\mathrm{Ma}}}{2}\right)^2\right)\cdot\gamma_{\mathrm{Ma}}}{\left((1/4)(1-X_{\mathrm{Ab}})(2-X_{Ab})^2\cdot\gamma_{\mathrm{Ab}}\right)^3} \quad \text{A6}$$

At equilibrium at a given P and T one has:

$$\Delta G_1 = 0 = \Delta G_1^{\mathrm{o}} + \mathrm{R}T\ln K_1 \quad \text{A7}$$

$$\Delta G_2 = 0 = \Delta G_2^{\mathrm{o}} + \mathrm{R}T\ln K_2 \quad \text{A8}$$

where ΔG is the Gibbs free energy of the reaction, $\Delta G°$ is the Gibbs free energy for the pure phases, R is the universal gas constant (kJ/K·mol), and T is temperature in Kelvins. Expressions A7 and A8 must be solved simultaneously to find the compositions of scapolite (X_{Ma}) and plagioclase (X_{Ab}) that satisfy both conditions for equilibrium. Values for $\Delta G°$ were calculated using the data in Table A1 and the expression:

$$\Delta G_{P,T}^{\mathrm{o}} = \Delta H_{1,298}^{\mathrm{o}} - T\Delta S_{1,298}^{\mathrm{o}} + \int_{298}^{T}\Delta C_P dT - T\int_{298}^{T}\left(\frac{\Delta C_P}{T}\right)dT + \Delta V_{1,298}^{\mathrm{o}}(P-P_0) \quad \text{A9}$$

Table A1. Thermochemical data used in this study from Holland and Powell (2011) and from Almeida and Jenkins (2017) for marialite.

Phase	$\Delta H°_{298\mathrm{K},\,1\mathrm{bar}}$ (kJ/mol)	$S°_{298\mathrm{K},\,1\mathrm{bar}}$ (kJ/K·mol)	$V_{298\mathrm{K},\,1\mathrm{bar}}$ (kJ/kbar·mol)	a*	b (x10^5)	c	d
albite(high)	-3921.49	0.2243	10.105	0.4520	-1.3364	-1275.9	-3.9536
halite	-411.3	0.0721	2.702	0.0452	1.797	0	0
marialite	-12167.49	0.75793	33.035	1.172	9.0626	-4676.4	-8.2379
anorthite	-4232.7	0.2005	10.0790	0.3705	1.001	-4339.1	-1.961
calcite	-1207.88	0.0925	3.6890	0.1409	0.5029	-950.7	-0.858
meionite	-13842	0.752	33.9850	1.359	3.6442	-8594.7	-9.598

* The heat capacity terms (a, b, c, and d) are the coefficients in the expression $C_P = a + b(\mathrm{T}) + c/(\mathrm{T}^2) + d/(\mathrm{T}^{0.5})$, and have units that give the heat capacity (C_P) in kJ/K·mol.

References Cited

Almeida, K. M. F., and Jenkins, D. M. (2017) Stability field of the Cl-rich scapolite marialiate. American Mineralogist, 102, 2484-2493.

Alt, J. C. (1995) Subseafloor processes in mid-ocean ridge hydrothermal systems. In: S. E. Humphris, R. A. Zierenberg, L. S. Mullineaux, and R. E. Thomson (eds) Seafloor hydrothermal systems: physical, chemical, biological, and geological interactions, Geophysical Monograph 91, American Geophysical Union, Washington D. C., 85-114.

Aranovich, L.Y., and Newton, R.C. (1996) H_2O activity in concentrated NaCl solutions at high pressures and temperatures measured by the brucite-periclase equilibrium. Contributions to Mineralogy and Petrology, 125, 200-212.

Baker, J., and Newton, R.C. (1995) Experimentally determined activity-composition relations for Ca-rich scapolite in the system $CaAl_2Si_2O_8$-$NaAlSi_3O_8$-$CaCO_3$ at 7 kbar. American Mineralogist, 80, 744-751.

Benisek, A., Kroll, H., Cemič, L., Kohl, V., Breit, U., and Heying, B. (2003) Enthalpies in (Na,Ca)- and (K,Ca)-feldspar binaries: a high-temperature solution calorimetric study. Contributions to Mineralogy and Petrology, 145, 119-129.

Boivin, P., and Camus, G. (1981) Igneous scapolite-bearing associations in the Chaine des Puys, Massif Central (France) and Atakor (Hoggar, Algeria). Contributions to Mineralogy and Petrology, 77, 365-375.

Ellis, D.E. (1978) Stability and phase equilibria of chloride and carbonate bearing scapolites at 750°C and 4000 bar. Geochimica et Cosmochimica Acta, 42, 1271-1281.

Eugster, H.P., and Prostka, H.J. (1960) Synthetic scapolites. Geological Society of America, 71, 1859-1860.

Evans, B.W., Shaw, D.M., and Haughton, D.R. (1969) Scapolite stoichiometry. Contributions to Mineralogy and Petrology, 24, 293-305.

Filiberto, J., Treiman, A.H., Giesting, P.A., Goodrich, C.A., and Gross, J. (2014) High-temperature chlorine-rich fluid in the martian crust: A precursor to habitability. Earth and Planetary Science Letters, 401, 110-115.

Fontaine, F. J., Wilcock, W. S. D., and Butterfield, D. A. (2007) Physical controls on the salinity of mid-ocean ridge hydrothermal vent fluids. Earth and Planetary Science Letters, 257, 132-145.

Giblin, L.E., Blackburn, W.H., and Jenkins, D.M. (1993) X-ray continuum discrimination technique for the energy dispersive analysis of fine particles. Analytical Chemistry, 65, 3576-3580.

Goldsmith, J.R. (1976) Scapolites, granulites, and volatiles in the lower crust. Geological Society of America, 87, 161-168.

Goldsmith, J.R., and Jenkins, D.M. (1985) The high-low albite relations revealed by reversal of degree of order at high pressures. American Mineralogist, 70, 911-923.

Goldsmith, J. R., and Newton, R. C. (1977) Scapolite-plagioclase stability relations at high pressures and temperatures in the system $NaAlSi_3O_8$-$CaAl_2Si_2O_8$-$CaCO_3$-$CaSO_4$. American Mineralogist, 62, 1063-1081.

Graziani, G., and Lucchesi, S. (1982) The thermal behavior of scapolites. American Mineralogist, 67, 1229-1241.

Hammerli, J., Spandler, C., Oliver, N. H. S., and Rusk, B. (2014) Cl/Br of scapolite as a fluid tracer in the earth's crust: insights into fluid sources in the Mary Kathleen Fold Belt, Mt. Isa Inlier, Australia. Journal of Metamorphic Geology, 32, 93-112.

680 Hammerli, J., Kemp, A. I. S., Barrett, N., Wing, B. A., Roberts, M., Arculus, R. J., Boivin, P.,
681 Nude, P. M., and Rankenburg, K., (2017) Sulfur isotope signatures in the lower crust: A
682 SIMS study on S-rich scapolite of granulites. Chemical Geology, 454, 45-66.
683 Hassan, I., and Buseck, P. R. (1988) HRTEM characterization of scapolite solid solutions.
684 American Mineralogist, 73, 119-134.
685 Holland, T. J. B., and Powell, R., 2011. An improved and extended internally consistent
686 thermodynamic dataset for phases of petrological interest, involving a new equation of state
687 for solids. Journal of Metamorphic Geology, 29, 333-383.
688 Jenkins, D. M. and Corona, J.-C. (2006) The role of water in the synthesis of glaucophane.
689 American Mineralogist, 91, 1055-1068.
690 Johnson, D.A., and Barton, M.D. (2000a) Field trip day four: Buena Vista Hills, Humboldt Mafic
691 Complex, Western Nevada. Society of Economic Geologists Guidebook Series, 32, 145-162.
692 Johnson, D.A., and Barton, M.D. (2000b) Time-space development of an external brine
693 dominated, igneous-driven hydrothermal system: Humboldt mafic complex, western Nevada.
694 Society of Economic Geologists Guidebook Series, 32, 127-143.
695 Johnson, E. L., Goergen, E. T., and Fruchey, B. L. (2004) Right lateral oblique slip movements
696 followed by post-Ottawan (1050-1020 Ma) orogenic collapse along the Carthage-Colton
697 shear zone: Date from the Dana Hill metagabbro body, Adirondack Mountains, New York.
698 In: Tollo, R.P., Corriveau, L., McLelland, J., and Bartholomew, M. J. (eds) Proterozoic
699 tectonic evolution of the Grenville orogeny in North America. Boulder Colorado, Geological
700 Society of America Memoir 197, 357-378.
701 Katongo, C., Koller, F., Ntaflos, T., Koeberl, C., and Tembo, F. (2011) Occurrence and origin of
702 scapolite in the Neoproterozoic Lufilian-Zambezi belt, Zambia: Evidence/role of brine-rich

fluid infiltration during regional metamorphism. In: J. Ray, G. Sen, and B. Ghosh (eds) Topics in Igneous Petrology, Springer Netherlands, 449-473, DOI: 10.1007/978-90-481-9600-5.

Kendrick, M. A., Arculus, R. J., Danyushevsky, L. V., Kamenetsky, V. S., Woodhead, J. D., and Honda, M. (2014) Subduction-related halogens (Cl, Br and I) and H_2O in magmatic glasses from Southwest Pacific backarc basins. Earth and Planetary Science Letters, 400, 165-176.

Kerrick, D.M., and Darken, L.S. (1975) Statistical thermodynamic models for ideal oxide and silicate solid solutions, with application to plagioclase. Geochimica et Cosmochimica Acta, 39, 1431-1442.

Kroll, H., and Ribbe, P. H. (1980) Determinative diagrams for Al,Si ordering in plagioclases. American Mineralogist, 65, 449-457.

Kullerud, K., and Erambert, M. (1999) Cl-scapolite, Cl-amphibole, and plagioclase equilibria in ductile shear zones at Nusfjord, Lofoten, Norway: Implications for fluid compositional evolution during fluid-mineral interaction in the deep crust. Geochimica et Cosmochimica Acta, 63, 3829-3844.

Larson, A.C., and Von Dreele, R.B. (2000) General Structure Analysis System (GSAS), Los Alamos National Lab Report (LAUR) 86-748.

Lieftink, D.J., Nijland, T.G., and Maijer, C. (1993) Cl-rich scapolite from Odegardens Verk, Bamble, Norway. Norsk Geologisk Tidsskrift, 73, 55-57.

Lovering, J. F., and White, A. J. R. (1964) The significance of primary scapolite in granulitic inclusions from deep-seated pipes. Journal of Petrology, 5, 195-218.

Makhluf, A.R., Newton, R.C., and Manning, C.E. (2016) Hydrous albite magmas at lower crustal pressure: new results on liquidus H_2O content, solubility, and H_2O activity in the system

$NaAlSi_3O_8$–H_2O–NaCl at 1.0 GPa. Contributions to Mineralogy and Petrology, 171, 75, 18pp, DOI 10.1007/s00410-016-1286-0.

Mora, C.I., and Valley, J.W. (1989) Halogen-rich scapolite and biotite: Implications for metamorphic fluid-rock interaction. American Mineralogist, 74, 721-737.

Newton, R.C., and Goldsmith, J.R. (1976) Stability of the end-member scapolites: $3NaAlSi_3O_8 \cdot NaCl$, $3CaAl_2Si_2O_8 \cdot CaCO_3$, $3CaAl_2Si_2O_8 \cdot CaSO_4$. Zeitschrift fur Kristallographie, 143, 333-353.

Oliver, N.H.S., Wall, V.J., and Cartwright, I. (1992) Internal control of fluid compositions in amphibolite-facies scapolitic calc-silicates, Mary Kathleen, Australia. Contributions to Mineralogy and Petrology, 111, 94-112.

Orville, P.M. (1975) Stability of scapolite in the system Ab-An-NaCl-$CaCO_3$ at 4 kb and 750°C. Geochimica et Cosmochimica Acta, 39, 1091-1105.

Oterdoom, W. H., (1979) Plagioclase-scapolite-calcite phase relations in high metamorphic argillaceous limestones. Schweizerische Mineralogische und Petrographische Mitteilungen, 59, 417-422.

Oterdoom, W.H., and Gunter, W.D. (1983) Activity models for plagioclase and CO_3·scapolites – An analysis of field and laboratory data. American Journal of Science, 283-A, 255-282.

Prewitt, C.T., Sueno, S., and Papike, J.J. (1976) The crystal structures of high albite and monalbite at high temperatures. American Mineralogist, 61, 1213-1225.

Price, J. G. (1985) Ideal site mixing in solid solutions, with an application to two-feldspar geothermometry. American Mineralogist, 70, 696-701.

747 Rebbert, C.R., and Rice, J.M. (1997) Scapolite-plagioclase exchange: Cl-CO_3 scapolite solution
748 chemistry and implications for peristerite plagioclase. Geochimica et Cosmochimica Acta,
749 61, 555-567.
750 Reed, S.J.B. (1996) Electron microprobe analysis and scanning electron microscopy in geology.
751 Cambridge University Press, Cambridge, United Kingdom.
752 Sokolova, E. and Hawthorne, F. C. (2008) The crystal chemistry of the scapolite-group minerals.
753 I. Crystal structure and long-range order. Canadian Mineralogist, 46, 1527-1554.
754 Sokolova, E.V., Kabalov, Y.K., Sherriff, B.L., Teertstra, D.K., Jenkins, D.M., Kunath-Fandrei,
755 G., Goetz, S., and Jäger, C. (1996) Marialite: Rietveld-structure refinement and ^{29}Si MAS
756 and ^{27}Al satellite transition NMR spectroscopy. Canadian Mineralogist, 34, 1039-1050.
757 Solberg, T. N., Abrecht, J., and Hewitt, D. A. (1981) Graphical procedures for the refinement of
758 electron microprobe analysis of fine-grained particles. In: R. H. Geiss (ed.) Microbeam
759 Analysis – 1981, San Francisco Press, 160-162.
760 Teertstra, D.K., and Sherriff, B.L. (1997) Substitutional mechanisms, compositional trends and
761 the end-member formulae of scapolite. Chemical Geology, 136, 233-260.
762 Teertstra, D. K., Schindler, M., Sherriff, B.L., and Hawthorne, F.C. (1999) Silvialite, a new
763 sulfate-dominant member of the scapolite group with an Al-Si composition near the *I*4/m-
764 $P4_2$/n phase transition. Mineralogical Magazine, 63, 321-329.
765 Vanko, D.A., and Bishop, F.C. (1982) Occurrence and origin of marialitic scapolite in the
766 Humboldt lopolith, N.W. Nevada. Contributions to Mineralogy and Petrology, 81, 277-289.
767 Yoshino, T., and Satish-Kumar, M. (2001) Origin of scapolite in deep-seated metagabbros of the
768 Kohistan Arc, NW Himalayas. Contributions to Mineralogy and Petrology, 140, 511-531.
769

770

771

This is a preprint, the final version is subject to change, of the American Mineralogist (MSA)
Cite as Authors (Year) Title. American Mineralogist, in press.
DOI: https://doi.org/10.2138/am-2019-6907

772

773 Table 1. Mixture bulk compositions, treatment conditions, and products of phase synthesis

774 experiments.

Sample Code	Bulk composition used	T (°C)	P (GPa)	t (h)	H_2O (wt%)	Products and comments
Scapolite ($Ma_{80}Me_{20}$) synthesis						
SSMF2-3	$Na_{2.4}Ca_{0.6}Al_{3.6}Si_{8.4}O_{24}$ + 6.8NaCl + 1.7$CaCO_3$	1030	1.80	23	0	scap, hal, cal
SSMF3-1	$Na_{2.4}Ca_{0.6}Al_{3.6}Si_{8.4}O_{24}$ + 6.4NaCl + 1.6$CaCO_3$	1030	1.80	23	0	scap, hal, cal
SSMF3-3	$Na_{2.4}Ca_{0.6}Al_{3.6}Si_{8.4}O_{24}$ + 6.4NaCl + 1.6$CaCO_3$	1030	1.80	20	0	scap, hal, cal, qtz
SSMF3-4	$Na_{2.4}Ca_{0.6}Al_{3.6}Si_{8.4}O_{24}$ + 6.4NaCl + 1.6$CaCO_3$	1030	1.80	20	0	scap, hal, cal, qtz
SSMF3-7	$Na_{2.4}Ca_{0.6}Al_{3.6}Si_{8.4}O_{24}$ + 6.4NaCl + 1.6$CaCO_3$	1030	1.80	20	0	scap, hal, cal
Plagioclase ($Ab_{80}An_{20}$) synthesis						
SSM1FP-1	3($Na_{0.8}Ca_{0.2}Al_{1.2}Si_{2.8}O_8$)	700	0.40	90	5.7	plag
SSM1FP-2	3($Na_{0.8}Ca_{0.2}Al_{1.2}Si_{2.8}O_8$)	700	0.40	91	7.2	glass - amorphous XRD pattern
SSM1FP-3	3($Na_{0.8}Ca_{0.2}Al_{1.2}Si_{2.8}O_8$)	700	0.40	90	2	neph, plag
SSM1-10*	3($Na_{0.8}Ca_{0.2}Al_{1.2}Si_{2.8}O_8$)	700	0.40	92	5.1	plag, cor, woll, neph
SSM1FP-4*	3($Na_{0.8}Ca_{0.2}Al_{1.2}Si_{2.8}O_8$)	700	0.40	92	5.6	plag
SSMF2-1	$Na_{2.4}Ca_{0.6}Al_{3.6}Si_{8.4}O_{24}$ + 6.8NaCl + 1.7$CaCO_3$	850	0.40	142	0	plag, hal, qtz, cal, cor
SSM1-1G	$Na_{2.4}Ca_{0.6}Al_{3.6}Si_{8.4}O_{24}$ + 1.6NaCl + 0.4$CaCO_3$	750	0.50	90	0	plag, qtz, cor, hal, cal
SSMF1G	$Na_{2.4}Ca_{0.6}Al_{3.6}Si_{8.4}O_{24}$ + 1.6NaCl + 0.4$CaCO_3$	750	0.50	90	0	plag, qtz, cor, hal, cal
SSMF3-2	$Na_{2.4}Ca_{0.6}Al_{3.6}Si_{8.4}O_{24}$ + 6.4NaCl + 1.6$CaCO_3$	800	0.55	67	0	plag, woll, scap, hal, cal
SSMF2-2	$Na_{2.4}Ca_{0.6}Al_{3.6}Si_{8.4}O_{24}$ + 6.8NaCl + 1.7$CaCO_3$	930	0.65	45	0	hal, plag, cal, cor
SSM1-1X	3($Na_{0.8}Ca_{0.2}Al_{1.2}Si_{2.8}O_8$)	800	1.00	45	0	qtz, plag, cor

SSMF1-10	$Na_{2.4}Ca_{0.6}Al_{3.6}Si_{8.4}O_{24}$ + 1.6NaCl + 0.4$CaCO_3$	900**	1.50	48	0	plag, qtz, hal, cal
SSM1-1P	$Na_{2.4}Ca_{0.6}Al_{3.6}Si_{8.4}O_{24}$ + 1.6NaCl + 0.4$CaCO_3$	900**	1.50	48	0	plag, qtz, hal, cal
SSM1F-1	3($Na_{0.8}Ca_{0.2}Al_{1.2}Si_{2.8}O_8$)	900**	1.50	45	0	plag, woll, qtz, cor

Note: Uncertainties are estimated at ± 15 °C in temperature and ± 0.05 GPa in pressure.

* Capsules were treated in the same experiment

** Heating ramp of 0.5 min used for these samples, all other at or above 1.0 GPa were 1 min

Abbreviations: cal = calcite; cor = corundum; hal = halite; neph = nepheline; plag = plagioclase; qtz = quartz; scap = scapolite; woll = wollastonite;

This is a preprint, the final version is subject to change, of the American Mineralogist (MSA)
Cite as Authors (Year) Title. American Mineralogist, in press.
DOI: https://doi.org/10.2138/am-2019-6907

783 Table 2. Compositions (average of *n* analyses) and unit-cell dimensions of the starting material
784 scapolite and plagioclase used to investigate the phase-equilibria in this study.

	Scapolite			Plagioclase			
Sample	SSMF3-1	SSMF3-3	SSMF3-7	SSM1F-1	SSM1FP-1	SSM1FP-4	SSM1-10
Composition (wt%)							
n	14	15	15	12	21	16	13
SiO_2	64.5(2.1)	64.5(2.5)	66.0(3.3)	69.6(1.5)	64.5(5.2)	64.9(3.7)	67.7(3.4)
Al_2O_3	20.0(1.7)	18.2(2.5)	17.9(2.6)	19.2(0.4)	22.3(3.4)	21.6(2.2)	20.9(2.6)
CaO	1.9(1.1)	1.2(1.0)	1.4(1.1)	0.23(1.7)	3.8(3.4)	2.7(2.0)	0.6(1.0)
Na_2O	9.1(0.7)	8.3(0.9)	8.2(0.8)	10.0(0.5)	8.9(1.9)	9.2(1.1)	10.9(0.8)
Cl	4.0(0.2)	4.0(0.3)	4.2(0.3)	0.01(0.01)	na	0.00(0.01)	0.01(0.01)
Total	99.6(1.9)	96.3(3.3)	97.7(2.5)	99.1(1.7)	99.6(1.8)	98.6(2.6)	100.2(1.6)
Total-O=Cl	98.7(1.9)	95.4(3.2)	96.7(2.5)				
Cations per Al + Si = 12				Cations per 8 oxygens			
Si	8.79(0.23)	9.01(0.34)	9.10(0.39)	3.04(0.02)	2.85(0.19)	2.89(0.12)	2.95(0.12)
Al	3.21(0.23)	2.99(0.34)	2.90(0.39)	0.99(0.01)	1.16(0.19)	1.13(0.12)	1.07(0.14)
Ca	0.28(0.17)	0.19(0.16)	0.21(0.16)	0.01(0.01)	0.18(0.16)	0.13(0.10)	0.03(0.05)
Na	2.41(0.19)	2.26(0.25)	2.20(0.23)	0.85(0.04)	0.76(0.15)	0.79(0.09)	0.92(0.06)
Cl	0.94(0.06)	0.96(0.07)	0.98(0.08)	0.00	na	0.00	0.00
Total	14.7(0.3)	14.45(0.26)	14.41(0.29)	4.89(0.03)	4.95(0.03)	4.94(0.03)	4.97(0.05)
Ca/(Ca+Na)	0.10(0.05)	0.08(0.06)	0.09(0.06)	0.01(0.01)	0.19(0.17)	0.14(0.10)	0.03(0.05)
Unit-cell dimensions							
a (Å)	12.054(1)	12.033(1)	12.035(1)	8.1433(8)	8.1599(9)	8.1506(7)	8.1490(7)
b (Å)	12.054(1)	12.033(1)	12.035(1)	12.853(1)	12.871(2)	12.858(2)	12.855(1)

c (Å)	7.5499(8)	7.5427(8)	7.5399(7)	7.1083(6)	7.1249(7)	7.1172(6)	7.1174(5)
α (°)	90.0	90.0	90.0	93.60(1)	93.55(1)	93.58(1)	93.65(1)
β (°)	90.0	90.0	90.0	116.43(1)	116.345(9)	116.36(1)	116.46(1)
γ (°)	90.0	90.0	90.0	89.94(1)	89.92(1)	89.89(1)	89.80(1)
V (Å^3)	1096.9(2)	1092.2(2)	1092.0(2)	664.62(7)	669.01(9)	666.73(7)	665.88(6)
t_1O - $<t_1m>$*	----	----	----	0.160	0.193	0.199	0.211
An (mol%)**	----	----	----	0.4(0.8)	10.8(1.4)	8.5(1.4)	0

Note: Standard deviations (1 σ) of the average of *n* analyses are given in parentheses for the compositional data, and in the last digit for the unit-cell dimensions.

* Tetrahedral Al-Si ordering parameter for plagioclase from Kroll and Ribbe (1980) based on the unit-cell angle γ: 0.0 = fully disordered; 1.0 = fully ordered (all Al at t_{1O}).

** Anorthite content derived from the least-squares regression of the β (°) values for the $C\bar{1}$ plagioclase data of Benisek et al. (2003) to a 3rd-order polynomial: An (mol%) = -1.3259 X 10^9 + 3.4226 X 10^7 * β - 2.9449 X 10^5 * β^2 + 8.4464 X 10^2 * β^3. Reported as 0 if calculated as less than 0.

794

795 Table 3. Synthetic phases used to make reversal mixtures for reactions (1) and (2) in the text.

Reversal mixture	Scapolite	Plagioclase	Halite*	Calcite*
REVSS1	SSMF3-1	SSM1F-1	3.2 moles	0.8 moles
REVSS2	SSMF3-3	SSM1FP-1	3.2 moles	0.8 moles
REVSS4	SSMF3-3	SSM1FP-4	4 moles	0.8 moles
REVSS5	SSMF3-7	SSM1-10	4 moles	0.8 moles

796 * Moles of halite or calcite per mole of scapolite
797

798

This is a preprint, the final version is subject to change, of the American Mineralogist (MSA)
Cite as Authors (Year) Title. American Mineralogist, in press.
DOI: https://doi.org/10.2138/am-2019-6907

799 Table 4. Treatment at dry conditions of reversal mixtures for reaction (1).

Sample code	T (°C)	P (GPa)	t (h)	Products and comments
REVSS2-15	650	0.40	70	no apparent reaction
REVSS2-10	750	0.40	96	scap, plag, hal, cal
REVSS2-12	500	1.50	44	plag, scap, hal, cal
REVSS2-16	550	1.50	46	no apparent reaction
REVSS2-17	580	1.50	46	no apparent reaction
REVSS2-14	600	1.50	46	no apparent reaction
REVSS2-18	620	1.50	46	plag, scap, hal, cal
REVSS2-19	630	1.50	23	no apparent reaction
REVSS2-11	650	1.50	45	scap, plag, hal, cal
REVSS1-6	650	2.00	44	plag, scap, hal, cal, woll
REVSS2-22	700	2.00	65	plag, scap, hal, cal
REVSS1-5	700	2.00	45	no apparent reaction
REVSS2-9	720	2.00	45	no apparent reaction
REVSS2-8	730	2.00	45	no apparent reaction
REVSS2-7	740	2.00	45	no apparent reaction
REVSS2-1	750	2.00	45	no apparent reaction
REVSS2-6	760*	2.00	45	scap, plag, hal, cal
REVSS2-4	780	2.00	47	scap, plag, hal, cal
REVSS2-5	780	2.00	66	scap, plag, hal, cal
REVSS2-3	800	2.00	22	scap, plag, hal, cal
REVSS1-4	800	2.00	22	scap, plag, hal, cal, woll

REVSS2-2	850	2.00	70	scap, plag, hal, cal
REVSS1-3	900	2.00	22	scap, hal, cal, woll
REVSS1-2	960	2.00	21	scap, hal, cal woll
REVSS1-1	1000	2.00	21	scap, hal, cal, woll

Note: Uncertainties are estimated as ± 5 °C in temperature and 0.05 GPa in pressure.

* Heating ramp of 0.5 min; all other experiments were done with a heating ramp of 1 min

This is a preprint, the final version is subject to change, of the American Mineralogist (MSA)
Cite as Authors (Year) Title. American Mineralogist, in press.
DOI: https://doi.org/10.2138/am-2019-6907

803
804 Table 5. Treatment at hydrothermal conditions of reversal mixtures for reaction (2).

Sample code	T (°C)	P (GPa)	t (h)	H_2O (wt%)	Products and comments
REVSS5-6	660	1.50	46	~5	scap, plag, hal, cal
REVSS5-4	660	1.50	46	~12	no apparent reaction
REVSS5-5	660	1.50	44	~15	plag, hal, cal
REVSS5-3	660	1.50	47	~27	plag, scap, hal, cal, qtz
REVSS5-1	680	1.50	45.5	~16	scap, plag, hal, cal
REVSS5-2	680	1.50	45	28	plag, hal, cal
REVSS5-8	700	1.50	45	7	scap, plag, hal, cal
REVSS5-7	700	1.50	40	13	plag, hal, cal
REVSS5-10	720	1.50	47	~7	scap, plag, hal, cal
REVSS5-9	720	1.50	46	12	scap, plag, hal, cal
REVSS2-20H	800	2.00	22	3	scap, hal
REVSS4-5	800	2.0	21	10	scap, hal
REVSS4-6	800	2.0	22	17	scap, hal, cal(?)
REVSS4-7	800	2.0	23	~28	plag, hal
REVSS4-1	830	2.0	23	6	scap, hal
REVSS4-2	830	2.0	22	10	scap, plag, hal, cal
REVSS4-3	830	2.0	20	18	scap, plag, hal, cal
REVSS4-4	830	2.0	20	28	plag, hal
REVSS4-10	850	2.0	21	~7	scap, hal
REVSS4-8	850	2.0	22	~14	plag, hal, cal

REVSS4-9	850	2.00	23	~25	plag, hal, cal

Note: All experiments were done with a heating ramp of 1 min. Uncertainties are estimated as ± 5 °C in temperature and 0.05 GPa in pressure.

Table 6. Compositions of scapolite synthesized at hydrothermal conditions in this study, reported as weight% oxides and chlorine and cations per 12 Al+Si atoms for the average of *n* electron microprobe analyses. Uncertainties (1σ) are given in parentheses.

Sample	REVSS4-3	REVSS4-6	REVSS4-10	REVSS5-1
Composition (wt%)				
n	5	12	14	10
SiO_2	58.5 (2.0)	57.5 (3.8)	57.4 (4.5)	59.6 (3.8)
Al_2O_3	19.3 (1.9)	20.4 (2.1)	20.3 (1.4)	19.5 (1.8)
CaO	2.64 (1.94)	3.85 (2.04)	4.25 (2.14)	3.21 (2.37)
Na_2O	12.2 (1.0)	12.0 (2.0)	11.8 (1.5)	12.6 (1.4)
Cl	4.06 (0.58)	3.15 (0.66)	3.81 (0.47)	3.37 (0.65)
Total	95.7 (2.5)	96.2 (4.5)	96.8 (3.8)	97.5 (2.6)
Total-O=Cl	94.8 (2.6)	95.5 (4.5)	95.9 (3.8)	96.8 (2.6)
Cations (per 12 Al+Si)				
TSi	8.65 (0.28)	8.46(0.32)	8.46 (0.30)	8.65 (0.36)
TAl	3.35 (0.28)	3.54(0.32)	3.54 (0.30)	3.35 (0.36)
Sum T	12	12	12	12
MCa	0.42 (0.30)	0.61(0.33)	0.68 (0.35)	0.51 (0.38)
MNa	3.50 (0.29)	3.41(0.31)	3.38 (0.32)	3.54 (0.33)
Sum M	3.92 (0.12)	4.02 (0.11)	4.06 (0.11)	4.05 (0.13)
Total	15.91 (0.13)	16.02(0.11)	16.06 (0.11)	16.05 (0.13)
Anions				
Cl	1.02 (0.16)	0.79 (0.17)	0.96 (0.13)	0.83 (0.16)
Ca/(Ca+Na)	0.11 (0.08)	0.15 (0.08)	0.17 (0.08)	0.12 (0.09)

821

822 Table 7. Compositions of plagioclase synthesized at hydrothermal conditions in this study,
823 reported as weight% oxides and cations per 8 O atoms of the average of *n* electron microprobe
824 analyses. Uncertainties (1σ) are given in parentheses.

Sample wt%	REVSS4-4	REVSS4-7	REVSS4-8	REVSS5-2
n	9	8	6	13
SiO2	69.1 (1.8)	64.5 (3.3)	61.1 (7.8)	67.1 (3.6)
Al2O3	20.8 (1.0)	19.6 (1.8)	19.5 (0.9)	21.0 (1.5)
CaO	1.67 (0.59)	1.81 (1.06)	2.09 (0.73)	2.08 (1.16)
Na2O	11.2 (0.5)	10.5 (1.0)	10.3 (1.3)	11.0 (1.0)
Total	102.7 (3.2)	96.4 (5.8)	93.0 (9.1)	101.3 (4.7)
Cations				
TSi	2.95 (0.03)	2.94 (0.05)	2.89 (0.09)	2.91 (0.06)
TAl	1.05 (0.03)	1.05 (0.05)	1.10 (0.10)	1.08 (0.06)
Sum T	4.00	3.99	3.99	3.99
MCa	0.08 (0.03)	0.09 (0.05)	0.11 (0.04)	0.10 (0.05)
MNa	0.92 (0.03)	0.92 (0.05)	0.94 (0.04)	0.93 (0.06)
Sum M	1.00 (0.03)	1.01 (0.06)	1.05 (0.04)	1.03 (0.05)
Total	5.00 (0.03)	5.01 (0.06)	5.03 (0.04)	5.01 (0.03)
X_{Ab}*	0.92 (0.02)	0.91 (0.05)	0.90 (0.04)	0.91 (0.05)
X_{Ab}**	0.95 (0.03)	0.93 (0.05)	0.90 (0.09)	0.90 (0.04)

825 * X_{Ab} = Na/(Na+Ca)

826 ** X_{Ab} = [(2-Al)+(Si-2)]/2

827

828
829 Figure captions

830 Figure 1. Representative back-scattered-electron (BSE) images. (a) Synthetic plagioclase
831 (unlabeled grains) from sample SSM1F-1. Minor wollastonite (W) is present as the brighter
832 grains, while rare quartz (Q) can be found, though nearly identical in grey-level brightness to
833 the plagioclase. (b) Image of the reversal starting mixture REVSS1, with the larger grains
834 labeled accordingly as plagioclase (P), scapolite (S), quartz, and wollastonite. All but the
835 wollastonite has very similar grey-level brightness. The scapolite tends to have a slightly more
836 regular blocky habit.

837 Figure 2. Compositions of starting material (solid symbols) and reaction product (open symbols)
838 phases, as determined by electron microprobe analysis, expressed in terms of the molar ratio of
839 Ca/(Ca+Na). (a) Scapolite compositions at 2.0 GPa (top) and 1.5 GPa (bottom). (b)
840 Plagioclase compositions at 2.0 GPa (top) and 1.5 GPa (bottom). Arrows indicate sense of
841 compositional re-equilibration from the starting materials (sample codes from Table 2 in
842 parentheses) to the final compositions for each of the reversal experiments indicated (REVSS
843 x-x).

844 Figure 3. *P-T* diagram of the experimental results of scapolite (Scap) stability (heavy solid line)
845 relative to plagioclase (Plag), halite (Hal), and calcite (Cal). Shown for comparison is the
846 stability of end-member marialite (Ma) from Almeida and Jenkins (2017, AJ 17, light solid and
847 dashed lines) relative to albite (Ab) and halite, as well as the curve for end-member marialite
848 from Filiberto et al. (2014, F 14, dash-dot curve). A significant shift in stabilization has
849 occurred with the small change in chemical composition from end-member marialite to
850 intermediate scapolite of the composition $Ma_{85}Me_{15}$. Open circles indicate growth of scapolite,
851 solid circles growth of plagioclase, and half-filled circles indicate no obvious reaction. Critical

data defining the stability of end-member marialite are from Almeida and Jenkins (2017), where the solid squares represent growth of marialite and the open squares growth of albite and either halite or, at low pressure, $NaCl_{liq}$ which is a liquid rich in NaCl, though not necessarily pure NaCl. The queried dashed line is a possible boundary indicating the lower-pressure stability of the intermediate scapolite of this study.

Figure 4. (a) Thermal stability of scapolite in the presence of water at 2.0 GPa, where X_{NaCl}^{Bulk} indicates the mole fraction of NaCl/(H_2O + NaCl) for the bulk mixture. Open circles indicate plagioclase growth, filled circles indicate scapolite growth, and half-filled circles indicate no reaction. Numbers indicate the (bulk) H_2O wt% used in that experiment. Estimated hydrothermal melting of NaCl ($NaCl_{liq}$) extrapolated from lower-pressure results of Aranovich and Newton (1996). Long horizontal line is the lower-thermal stability of scapolite from Figure 3 incorporated into this diagram. (b) Stability of scapolite in the presence of water at 1.5 GPa. Possible minimum salinities of the brine before scapolite breaks down to plagioclase + calcite + liquid are shown as maximum (Max) and minimum (Min) at approximately 0.32 and 0.15 X_{NaCl}^{Bulk}, respectively. Other abbreviations and symbols as in (a).

Figure 5. (a) Chlorine contents in atoms per formula unit (apfu) vs mole fraction Ca/(Ca+Na+K) for scapolite by electron microprobe analysis of phases from this study (solid squares) and from natural samples: circles are from the Humboldt lopolith, Nevada (Vanko and Bishop, 1982; VB 1982); diamonds are from various localities reported in Graziani and Luchessi (1982; GL 1982); triangles are from the calc-silicates of the Mary Kathleen fold belt, Australia (Oliver et al.,1992; OWC 1992); dash-circles are from scapolitized metagabbros of the Bamble Sector, Norway (Lieftink et al., 1993; LNM 1993); hexagons are from scapolite-bearing calc-silicates of the Wallace Formation, Idaho (Rebbert and Rice, 1997; RR 1997); stars are

scapolites from various localities (Teertstra and Sherriff, 1997; TS 1997); pluses are from a sheared gabbro-anorthosite in Lofoten, Norway (Kullerud and Erambert, 1999; KE 1999); crosses are from the Dana Hill metagabbro, New York (Johnson et al., 2004; JGF 2004); and squares are scapolite in a melt inclusion in the meteorite Nakhla (Filiberto et al, 2014; F et al 2014). Diagonal lines join ideal marialite (Ma) with mizzonite or with meionite (Me). (b) Chlorine contents (apfu) vs (Si-6)/3 for synthetic and natural scapolites. Same symbols as in (a). Diagonal lines join Ma and Me, mizzonite (Miz) and Ma, and Me and dipyre ($Na_3CaAl_4Si_8O_{24}Cl$).

Figure 6. Comparison of the lower-thermal stability of the intermediate scapolite from this study ($Ma_{85}Me_{15}$) with that of end-member marialite ($Ma_{100}Me_0$) from Almeida and Jenkins (2017, AJ 2017) and meionite (Ma_0Me_{100}) from Goldsmith and Newton (1977, GN 1977).

Figure 7. (a) Calculated phase equilibria for scapolite (Scap), shown by filled symbols, coexisting with albitic plagioclase (Ab_{ss}) or anorthitic plagioclase (An_{ss}), shown by open symbols. Curves calculated using asymmetric or two-parameter Margules treatment as discussed in the text. Interaction parameters (W_{Ma}, W_{Me}) were calibrated to the two data points (circles) from this study. (b) Calculated phase equilibria as in (a) but with interaction parameters calibrated to the approximate compositions of coexisting Ab_{ss} and scapolite taken from the literature. Samples or compositional ranges are from Oterdoom (1979 = Ot 1979, diamonds), Rebbert and Rice (1997 = RR 1997, triangles), Johnson et al. (2004 = JGF 2004, squares), and Katongo et al. (2011= K et al. 2011, hexagons). All assemblages are in the presence of excess halite and calcite.

This is a preprint, the final version is subject to change, of the American Mineralogist (MSA)
Cite as Authors (Year) Title. American Mineralogist, in press.
DOI: https://doi.org/10.2138/am-2019-6907

897 Figure 1.

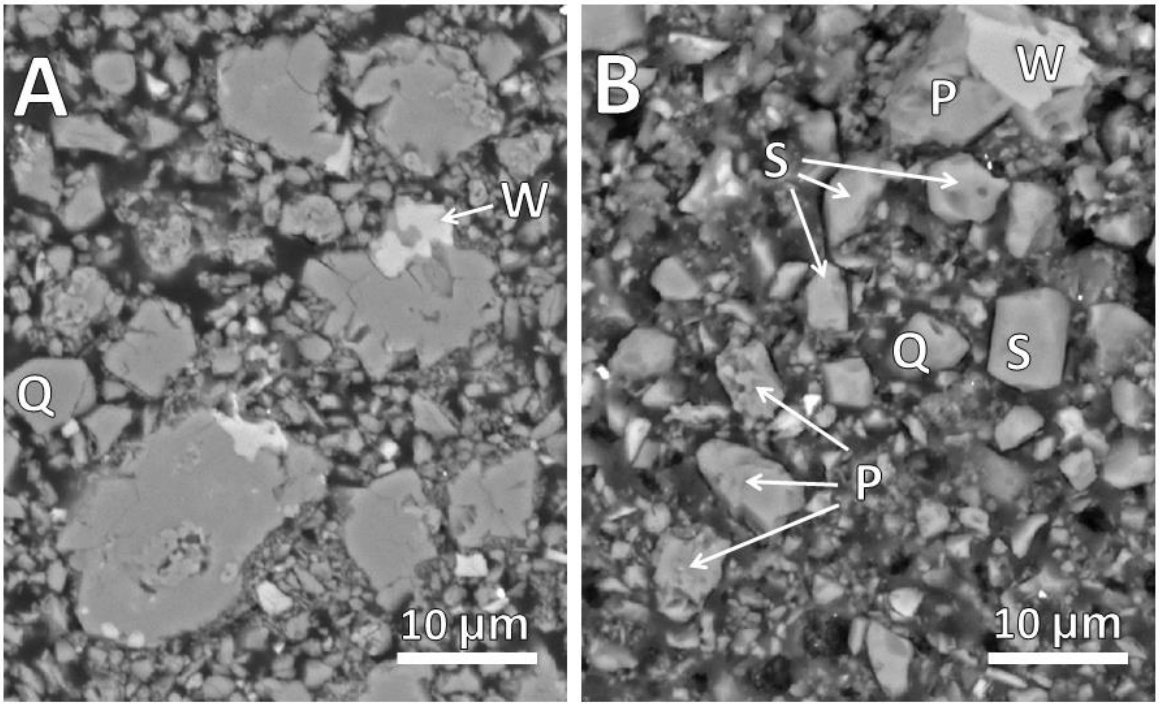

898

This is a preprint, the final version is subject to change, of the American Mineralogist (MSA)
Cite as Authors (Year) Title. American Mineralogist, in press.
DOI: https://doi.org/10.2138/am-2019-6907

899 Figure 2.

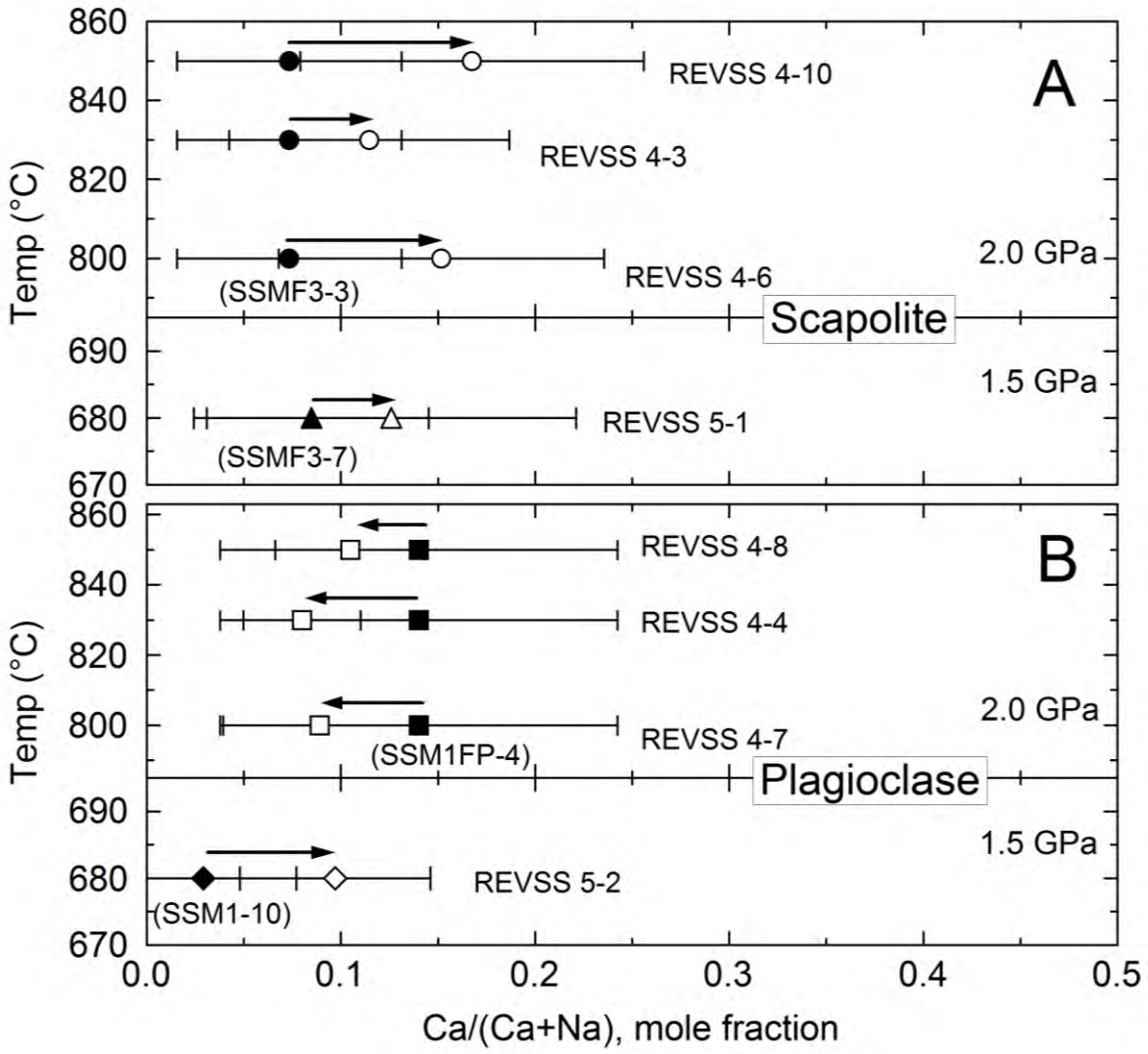

900
901
902

This is a preprint, the final version is subject to change, of the American Mineralogist (MSA)
Cite as Authors (Year) Title. American Mineralogist, in press.
DOI: https://doi.org/10.2138/am-2019-6907

903 Figure 3.
904

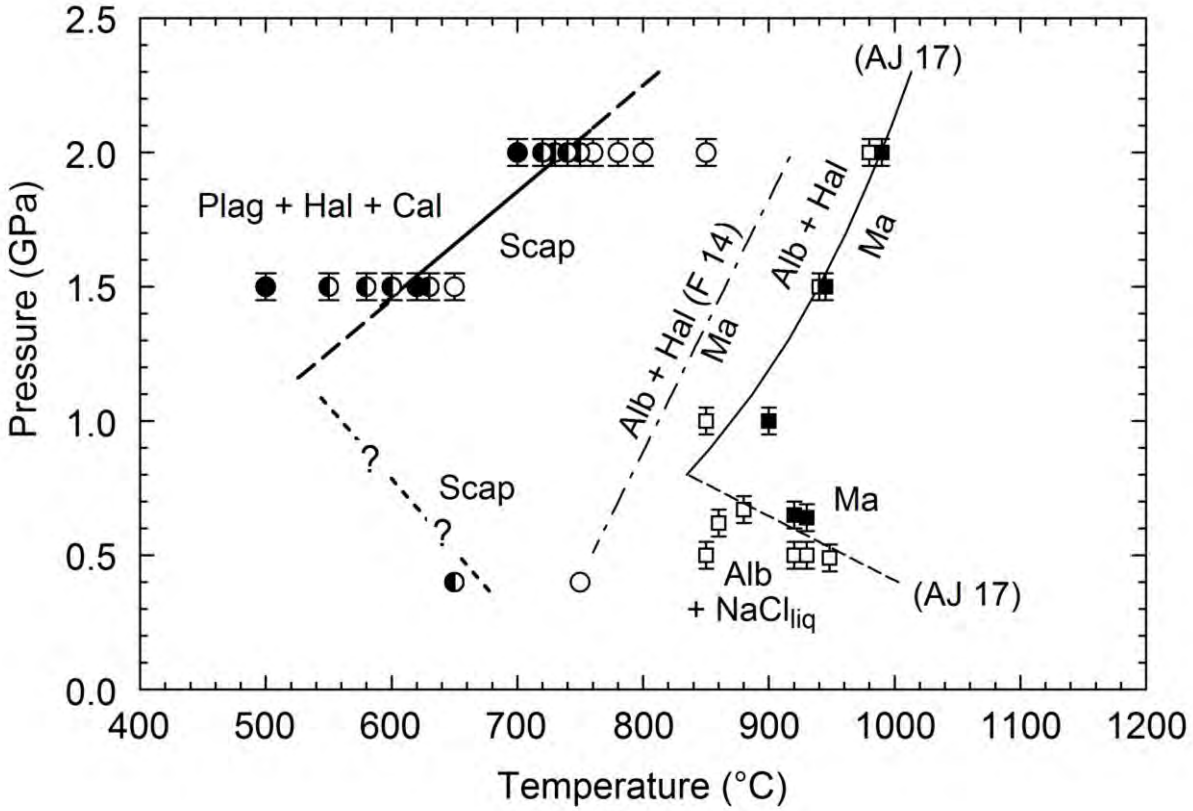

905
906
907

This is a preprint, the final version is subject to change, of the American Mineralogist (MSA)
Cite as Authors (Year) Title. American Mineralogist, in press.
DOI: https://doi.org/10.2138/am-2019-6907

908
909 Figure 4.

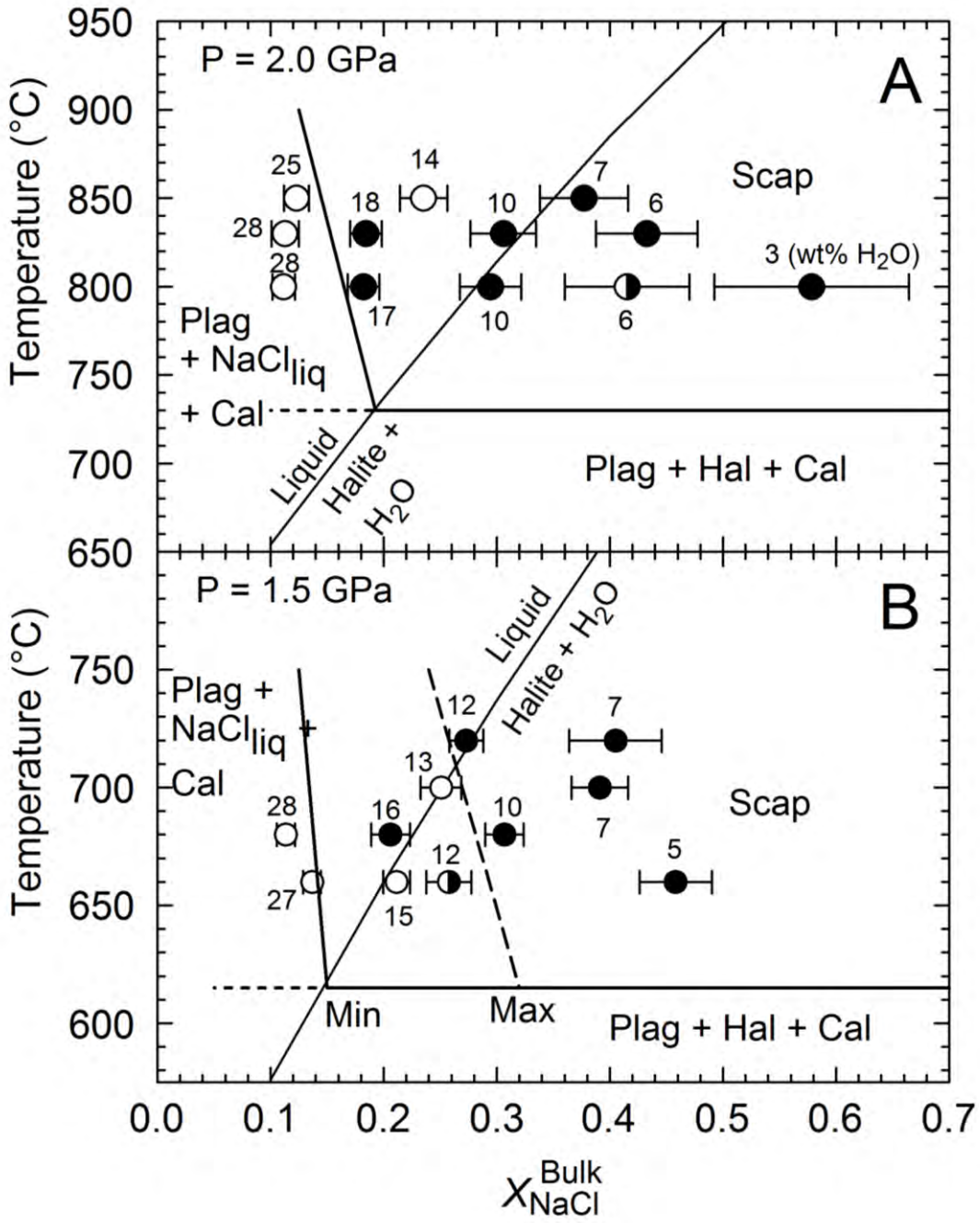

910
911
912

This is a preprint, the final version is subject to change, of the American Mineralogist (MSA)
Cite as Authors (Year) Title. American Mineralogist, in press.
DOI: https://doi.org/10.2138/am-2019-6907

913 Figure 5.

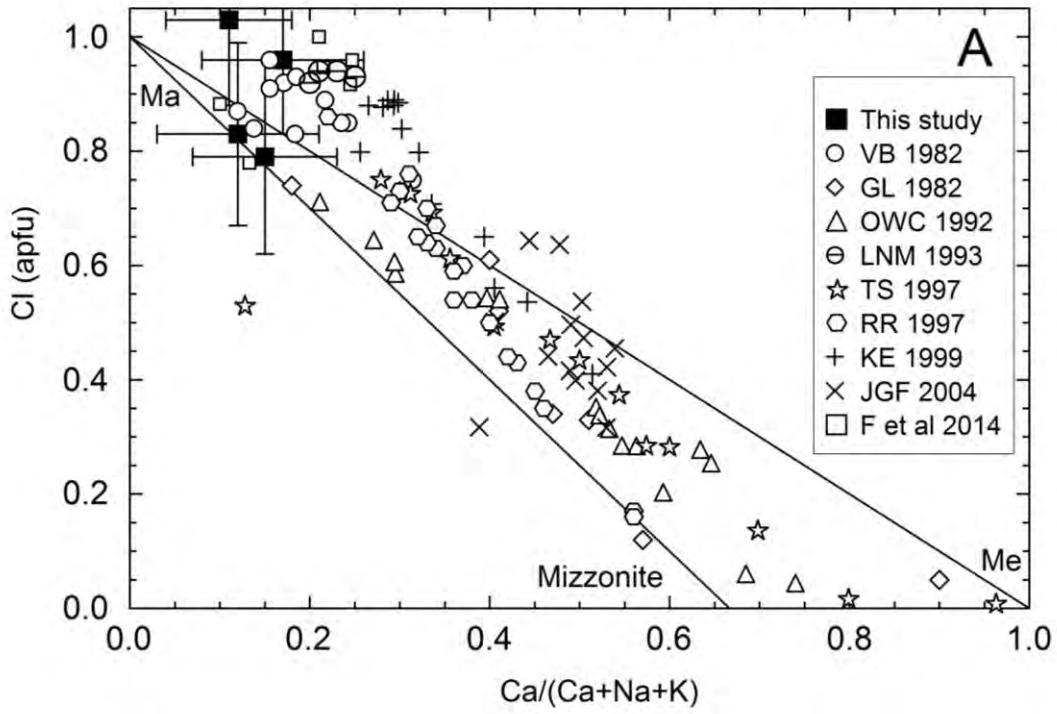

914
915

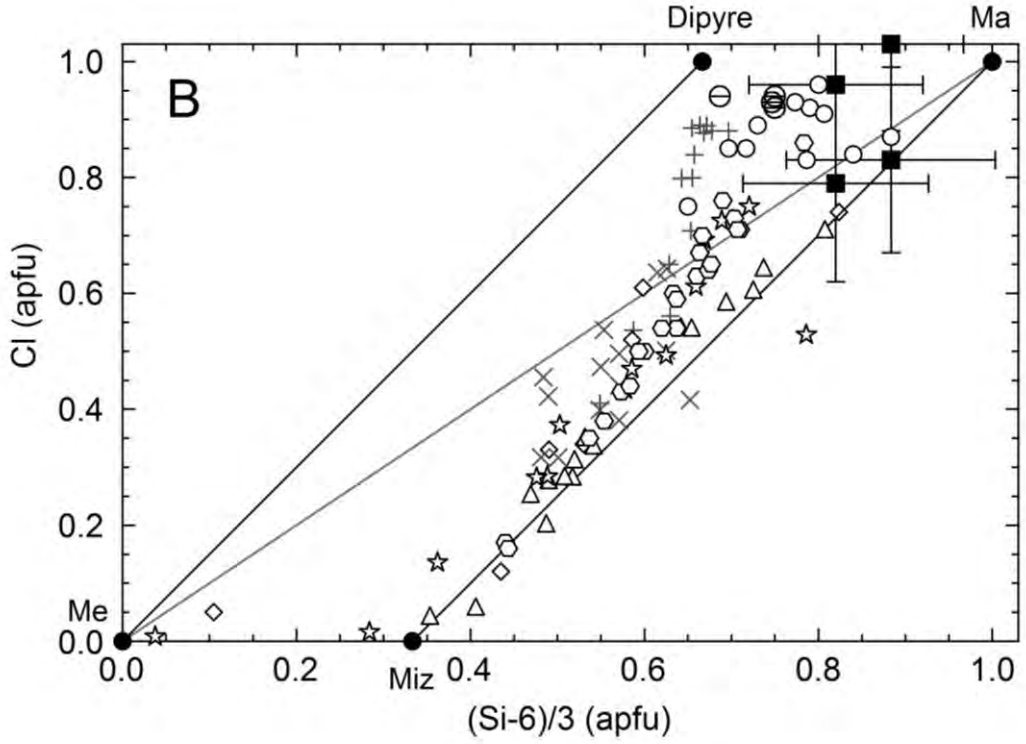

916

This is a preprint, the final version is subject to change, of the American Mineralogist (MSA)
Cite as Authors (Year) Title. American Mineralogist, in press.
DOI: https://doi.org/10.2138/am-2019-6907

Figure 6.

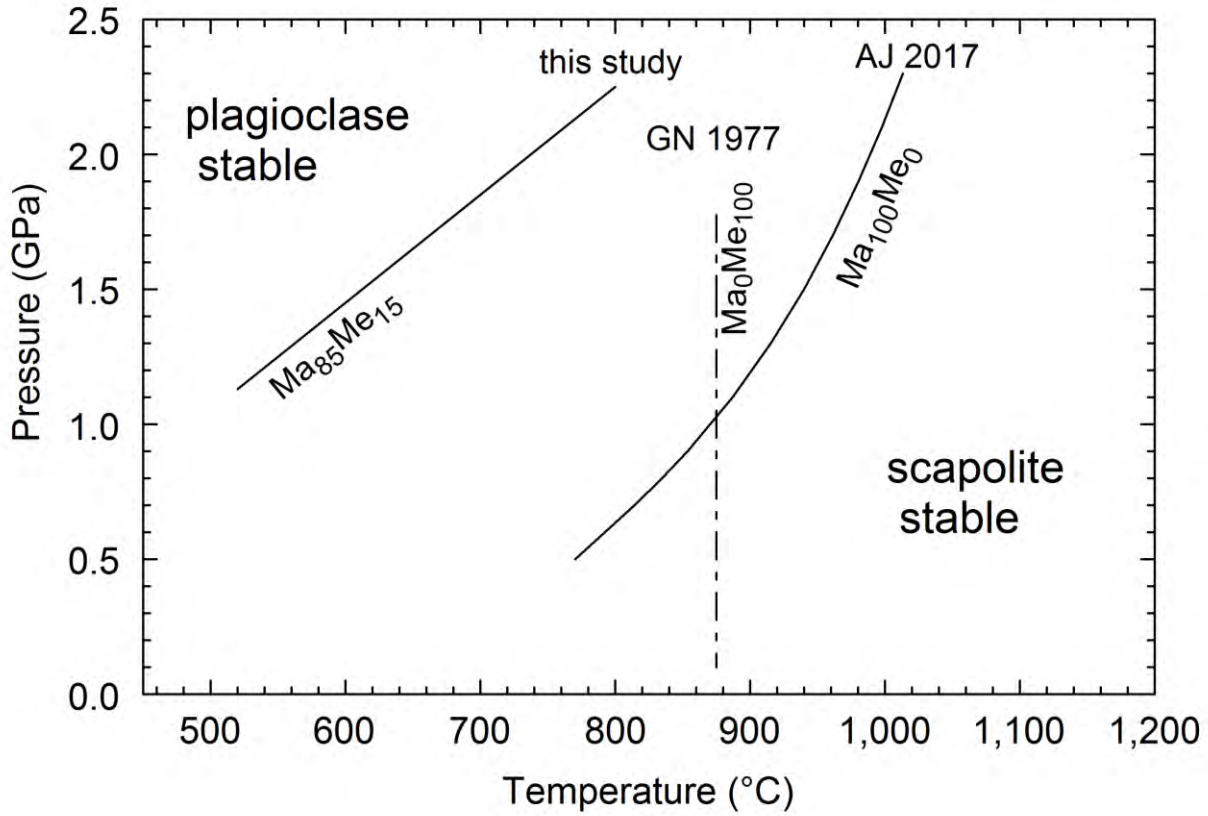

This is a preprint, the final version is subject to change, of the American Mineralogist (MSA)
Cite as Authors (Year) Title. American Mineralogist, in press.
DOI: https://doi.org/10.2138/am-2019-6907

922
923
924 Figure 7.

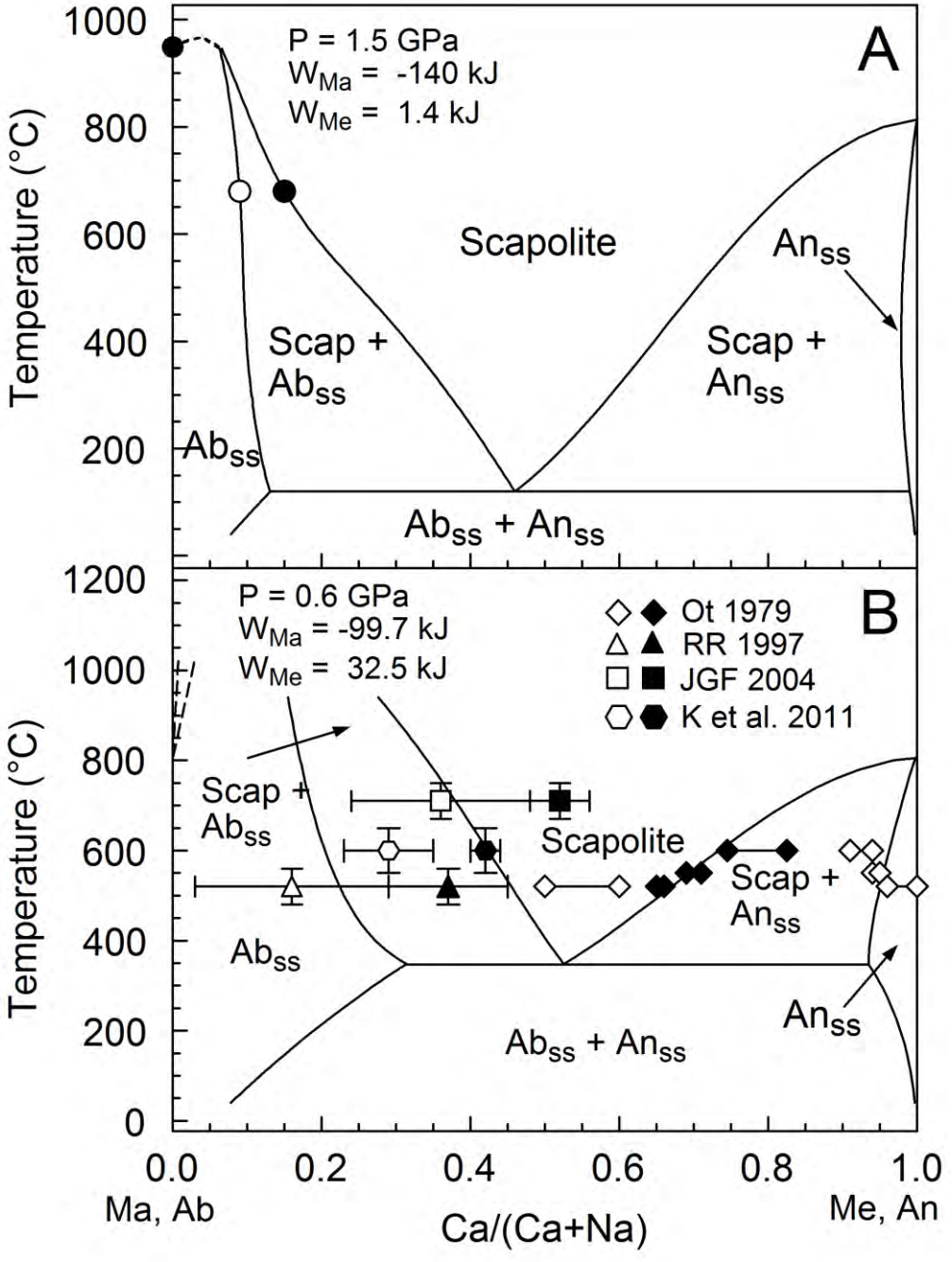

925